Chemical Science

ROYAL SOCIETY OF CHEMISTRY

REVIEW

View Article Online
View Journal

Cite this: DOI: 10.1039/d5sc09456a

From light loss to light harvesting: anti-reflective coatings bridging optics, materials, and performance in perovskite solar cells

Sonia Rani, Silvia Cavalli and Giulia Grancini *

Anti-reflective coatings (ARCs) are critical for maximizing photon harvesting in perovskite solar cells (PSCs) by mitigating reflection losses and enhancing photocurrent generation. Despite widespread documentations of ARCs in various optoelectronic fields, their integration into PSCs remains relatively underexplored. This review offers a comprehensive overview of the design, development, and optimization of ARCs specifically tailored for PSCs. We begin by outlining the unique optical and structural challenges in PSC architectures that make conventional ARCs less effective to PSCs. Various types of ARCs including monolayer, multilayer, graded refractive index, nanostructured or surface-textured ones, and spectral down-conversion coatings are explored alongside their fabrication methodologies. Beyond optical performance, we emphasize critical practical considerations such as anti-soiling properties, infrared management, mechanical robustness, and thermal stability, which are essential for ARC real-world deployment. Additionally, we underscore the role of optical Modeling techniques in fine-tuning the ARCs to optimize spectral and angular photon management within PSCs. By bridging fundamental principles with practical requirements, this review highlights the immense potential of ARC technologies to significantly improve light absorption, current density (J_{sc}), and ultimately the efficiency of PSCs.

Received 3rd December 2025
Accepted 20th February 2026

DOI: 10.1039/d5sc09456a

rsc.li/chemical-science

1. Introduction

Increasing demand for efficient and sustainable energy solutions has driven significant advancements in the solar energy

Department of Chemistry, INSTM, University of Pavia, Via T. Taramelli 14, 27100 Pavia, Italy. E-mail: giulia.grancini@unipv.it

Sonia Rani

Sonia Rani received a PhD in Physics from the Indian Institute of Technology (IIT) Dharwad, India, where the doctoral research focused on the design and experimental realization of advanced photonic structures for multifunctional perovskite solar cell applications. The work primarily addressed the designing and fabrication of transparent electrodes, photonic crystals and their multi-functionality in bifacial and colored perovskite solar cells. Following the PhD, Sonia Rani joined the University of Pavia as a postdoctoral researcher in the research group of Prof. Giulia Grancini. Current research interests include photonic and optoelectronic engineering of next-generation perovskite photovoltaics, light-management nanostructures, for high-performance and stable solar energy technologies.

Silvia Cavalli

Silvia Cavalli obtained her Master's Degree in Chemistry (2002) from the University of Milan in Italy and her PhD (2006) under the direct supervision of Prof. Dr Alexander Kros at Leiden University, The Netherlands. During her research experience, she worked on different interdisciplinary projects related to the field of nanotechnology (from synthetic and physical chemistry to biology). She recently joined Prof. Giulia Grancini's group at the University of Pavia as a Research Technologist, where she is currently involved in developing routes for Efficient and Sustainable Perovskite Solar Cells exploiting "Smart" Materials.

field over the past two decades.[1] Various photovoltaic (PV) technologies, including dye-sensitized, silicon-based, and organic solar cells, have already demonstrated strong potential to address global energy requirements, but still there is a need for next-generation materials that offer enhanced performance, lower production costs, and greater functional versatility, such as mechanical flexibility, semitransparency, colour tunability, and simplified fabrication processes.[2–7] While the commercial PV market has long been dominated by crystalline silicon solar cells, the emergence of perovskite solar cells (PSCs) marks a major shift in the PV sector. PSCs with power conversion efficiencies (PCEs) now exceeding 26% have positioned themselves at the forefront of cutting-edge PV research and development.[8,9] PSCs are a multilayer device stack, where each layer serves a specific and crucial function in determining overall device performance. This intricate architecture leads to PSC unique optoelectronic properties and supports its record-breaking efficiency improvements.[10–12] While notable progress has been made in boosting PSC performance through material innovation, interface engineering, and processing techniques, these approaches often require complex and time-intensive protocols.[13–15] In contrast, light management strategies present a more accessible and scalable route to further improve device efficiency, particularly by enhancing photon utilization and reducing optical losses.[16] Several methods can be adopted to perform light management in PSCs, including surface texturing for improved light trapping, the use of back reflectors, and the introduction of optical layers within the device architecture to enhance photon coupling.[17] These optical layers increase light absorption through microcavity effects (an interference phenomena that improve the optical field distribution within the photoactive layer).[18] Additionally, nanostructures can manipulate light propagation by creating optical resonances and plasmonic effects, which reduce parasitic absorption, therefore, plasmonic approaches, particularly those exploiting surface plasmon resonance, offer a powerful mechanism for enhancing light harvesting *via* strong near-field confinement and localized electromagnetic field enhancement.[19] Another effective approach is the incorporation of anti-reflection coatings (ARCs), which minimize reflection losses at the air/substrate interfaces within the solar cell. Among these light management techniques, ARCs stand out as a simple yet powerful approach to reduce reflection losses, thereby enhancing light absorption and increasing the photocurrent density (J_{sc}) of the device. In fact, many of the above-mentioned methods such as surface texturing, nanostructures, and optical layers, can be viewed as specialized types or subcategories of ARCs, all aimed at managing reflection losses effectively. Since PSCs are multilayer structures, the refractive indices of individual layers play a crucial role in governing optical phenomena like transmission, reflection, absorption, and scattering within the device. Fig. 1 illustrates light propagation through single-layer and multilayer thin-film ARCs, highlighting their role in minimizing reflection losses.

Although extensive research has been conducted to develop ARCs for broad-spectrum applications, including silicon PV technology, optical lenses, and display screens yet the integration of ARCs within PSC architectures necessitates careful consideration of several key factors.[20] Since the intensity of incident light reaching the active layer (light absorbing layer) is strongly influenced by the refractive indices of the intervening layers. Consequently, ARCs optimized for bare glass substrates often exhibit suboptimal performance when applied to PSCs. Specifically, the refractive indices of transparent conductive oxides (TCOs), such as indium tin oxide (ITO) and fluorine-doped tin oxide (FTO), as well as flexible substrates including polyethylene naphthalate (PEN) and polyethylene terephthalate (PET), significantly alter the optical environment, impacting the light coupling efficiency (the optical profile compared to bare

Giulia Grancini

Giulia Grancini is full professor at the Chemistry Department of the University of Pavia, leading the PVsquared2 team and several international project, such as the ERC Consolidator Grant "ELOW-DI" for the development of low-dimensional perovskite solar cells for indoor applications, and previously the ERC Starting Grant "HY-NANO" and the ERC POC "Spike", developing advanced hybrid perovskites solar cells. She obtained her PhD in physics from Politecnico di Milano in 2012 and worked as a postdoc researcher at IIT in Milano. From 2015 to 2019, she joined the EPFL awarded by SNSF with the Ambizione Energy Grant. Since 2019, she has been among the highly cited scientists from Web of Science with h-index of 57 and more than 24,000 citations. She also co-coordinates the EU project GoPV, a large European consortium focused on perovskite photovoltaics. She has been appointed "Cavaliere della Repubblica" for scientific merits by the President Mattarella. More information can be found at ***https://pvsquared2.unipv.it****.*

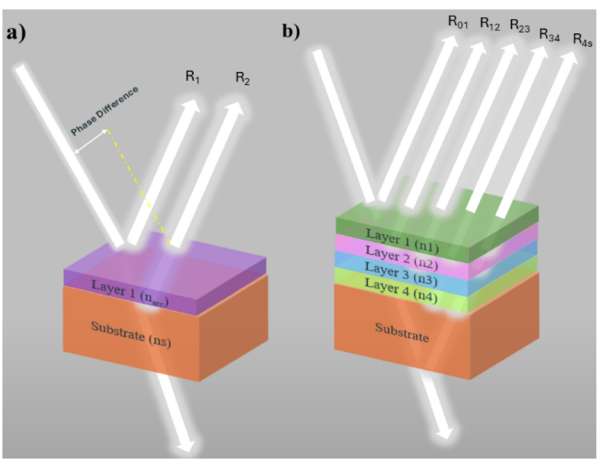

Fig. 1 Role of anti-reflective coatings (ARCs) in minimizing reflection losses: (a) Single-layer ARC, (b) multilayer ARC.

glass) thus, necessitating ARC designs tailored to specific configurations.

While silicon-based solar cells continue to dominate the commercial PV market, the momentum toward the commercialization of PSCs is rapidly accelerating. Companies such as Oxford PV and Saule Technologies are actively advancing perovskite technologies toward real-world applications.[21,22] However, as this transition progresses, it becomes increasingly important to understand and optimize ARCs specifically designed for PSCs.[23] Since the PSCs have their unique optical and structural properties,[10,12] thus set them apart from the conventional PV systems. As a result, ARCs developed for traditional silicon-based solar cells could not translate that high improvement to PSC devices. Thus, there is a need for a targeted literature study that points out the knowledge gaps and directs future research toward optimizing light management solutions designed especially for PSCs. This review aims to fill that gap by providing a comprehensive overview of ARC integration in PSCs, covering material selection, design strategies, Modeling techniques, fabrication methods, and performance metrics. It highlights the crucial role ARCs play in enhancing the optical and electrical performance of next-generation PSCs.

Importantly, we also discuss how the functional performance of ARCs varies under different ambient conditions, such as UV exposure, humidity, mechanical abrasion, and dust accumulation, highlighting the real-world relevance of coating design. The review further explores how optical modeling and machine learning approaches can be useful to predict ARC performance, optimise multifunctional coatings, and guide future research in designing robust, high-performance ARCs for PSCs. Additionally, this review systematically addresses the trade-offs associated with multifunctional ARCs for instance, combining anti-reflection, self-cleaning, hydrophobicity, or photocatalytic properties and how these functionalities impact optical transmittance, mechanical durability, and long-term stability. By presenting this structured and critical perspective, the review not only summarizes existing knowledge but also provides practical insights and forward-looking guidance for the research community, offering value beyond prior reviews.

2. Key aspects for ARCs for PSCs

To design an effective ARC for PSCs, several critical factors must be carefully considered to ensure optimal device performance and durability. Firstly, the ARC should exhibit broadband anti-reflective properties, minimizing reflection losses across a wide spectrum of wavelengths relevant to solar irradiation.[24,25] This ensures maximum light harvesting and improves overall power conversion efficiency (PCE). Additionally, the ARC must possess robust thermal and mechanical stability to withstand the varying environmental stresses encountered during device operation, including temperature fluctuations, humidity, and mechanical wear.[26–29] Thermal management is particularly important for PSCs due to their sensitivity to heat. Therefore, ARCs with infrared (IR) reflective capabilities are desirable to reduce heat buildup within the device, thereby enhancing operational stability and lifetime.[30] Beyond optical and thermal

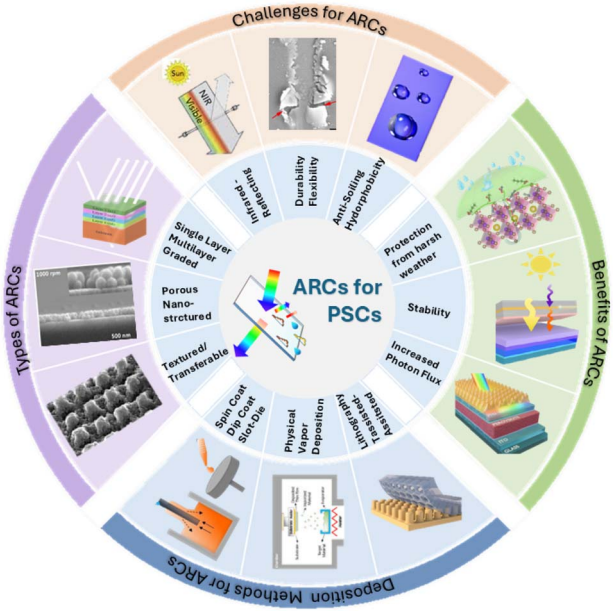

Fig. 2 Overview of the characteristics of an effective ARC for PSCs. Reproduced from ref. 17, 34–42 and 102 with permission.

performance, ARCs should also exhibit anti-soiling characteristics to maintain high efficiency over time. Hydrophobic surfaces that repel dust, water droplets, and other contaminants can prevent soiling and reduce maintenance requirements.[31–33] Incorporating these self-cleaning functionalities further ensures sustained optical clarity and performance without frequent manual cleaning. Importantly, these ARC properties must be validated on substrates identical or highly representative of those used in PSC fabrication, such as TCOs or flexible polymer films, to accurately assess their real-world effectiveness. Moreover, the fabrication methods for ARCs should be compatible with existing PSC manufacturing processes, favouring scalable, low-temperature, and cost-effective deposition techniques. Fig. 2 provides a schematic overview of the key topics discussed in this review, including ARC classification, essential performance characteristics, various deposition techniques, and the major challenges that must be addressed to advance ARC integration in PSC technology.[17,34–42]

3. Progress and limitations of ARCs existing in the literature for PSCs

Numerous studies in literature have focused on the development of effective ARCs, yet several critical factors must be addressed for their successful implementation. For instance, the fabrication methods employed may not be compatible with all device architectures (rigid or flexible devices), and the resulting ARCs may lack thermal stability at elevated temperatures, resulting in a change in the optical characteristics. Additionally, mechanical robustness remains a crucial consideration for practical applications of the ARCs in real-world environmental conditions.[43]

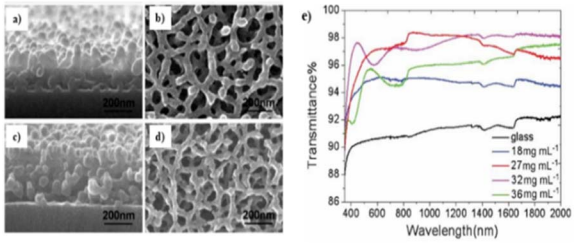

Fig. 3 (a)–(c) showing the cross-SEM images of nanoporous polymer ARC,[25] (b)–(d) showing their respective surface morphology,[25] (e) transmittance spectra of glass with and without the ARC. Reproduced from ref. 25 with permission from Wiley, copyright 2010.

Li *et al.*[25] in their work developed a gradient refractive index structure based on omnidirectional ARCs (that are designed to minimize reflection and maximize light transmission over a wide range of angles of incidence) by blending polystyrene-*block*-poly(methyl methacrylate) (PS-*b*-PMMA) with PMMA. This blend yielded an omnidirectional ARC that improved the average transmittance of a bare glass substrate by approximately 4%. Fig. 3(a) through 3(d) depict cross-sectional and surface morphology SEM images of porous polymer ARCs at varying solvent concentrations, while Fig. 3(e) presents the transmittance spectra of the glass substrate with and without the nanoporous ARC. However, a significant limitation of this approach is the poor thermal stability of the PS polymer at elevated temperatures, which compromises its mechanical integrity.[44] Since the annealing process of perovskite films typically occurs between 100 °C and 150 °C to evaporate solvents, the polymer inability to withstand these temperatures can degrade its nanostructure, alter its optical properties, and potentially lead to suboptimal device performance.[45] Moreover, as previously discussed, the refractive index of the substrate layers strongly influences ARC performance.

Hence, ARCs optimized for bare glass substrates may not function effectively on TCO-coated glass due to differences in refractive index values. Similarly, Ruud *et al.*[46] designed an ARC through a co-sputtering technique involving SiO_2 and ZnO, followed by annealing and etching in dilute hydrochloric acid to create a nanoporous SiO_2 network. Fig. 4(a) illustrates the concept of forming a nanoporous SiO_2 ARC *via* co-sputtering. Fig. 4(b) shows the change in transmittance spectra of fused glass substrates coated on both sides with the optimized ARC, while Fig. 4(c) presents the refractive index and thickness variations of the ARC at elevated temperatures. By controlling the etching percentage, they successfully modified the refractive index of the SiO_2 ARC, achieving an average visible transmittance (AVT) of 95% when applied to both sides of fused silica glass. Nonetheless, this method is limited to glass substrates, as refractive index tuning occurred only at annealing temperatures between 750 °C and 850 °C. Such high temperatures are incompatible with the thermal stability of the TE materials, which degrade under these conditions. Additionally, the dilute HCl etching process poses risks to TCO layers on coated substrates, rendering this approach unsuitable for PSC applications. Table 1 summarizes various ARCs reported in the literature alongside their primary limitations that preclude their effective use in PSC configurations. But it is important to highlight that although these ARCs may not be ideally suited for PSC applications in their current form, they demonstrated effectiveness in other areas, such as crystalline silicon solar cells, dye-sensitized solar cells (DSSCs), and organic photovoltaics (OPVs), underscoring their broader potential in optoelectronics applications. With further research, these coatings can be tailored or engineered to overcome current limitations, enabling their adaptation and optimization for PSC technologies.

In this section, we examined several existing ARC technologies that are not well suited to PSC architecture due to specific optical and structural limitations. In the following section, we focus on ARC strategies reported in the literature that have been effectively adapted and integrated into PSC configurations while discussing the benefit of each type of ARCs.

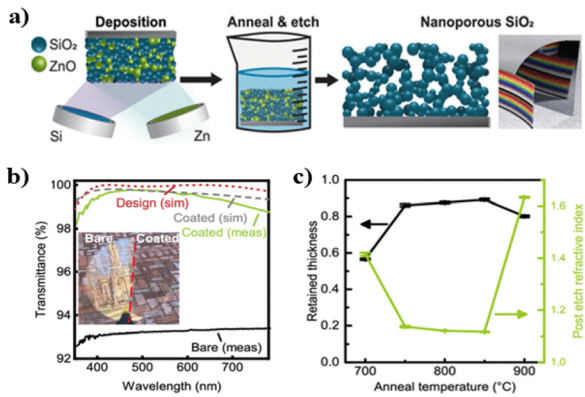

Fig. 4 (a) Overview of the formation of the nanoporous SiO_2 film *via* co-sputtering of Si and Zn. (b) Transmittance spectra of fused silica substrate with and without the ARC, (c) variation in the refractive index and the thickness of the ARC at various annealing temperatures. Reproduced from ref. 46 with permission from ACS publications, copyright 2022.

4. Classification of ARCs for PSCs

Building upon the discussion of the critical role ARCs play in enhancing the optical and overall performance of PSCs, this section delves into the various types of ARCs that have been explored specifically for perovskite devices. We have previously addressed the underlying design principles, material considerations, and the influence of optical and environmental factors on ARC performance. Now, we shift our focus to categorizing and analysing the different ARC architectures that have been reported in the literature in the context of PSC integration. Based on their structural and functional design, ARCs for PSCs can be broadly classified into four main categories, which are (1) Planar and Graded-Index ARCs, (2) Porous ARCs, (3) Texture and Transferable ARCs, and (4) Photonic Down-conversion-based ARCs. Each of these types of ARCs offers distinct optical properties and advantages, depending on their structural configuration, fabrication techniques, and compatibility with the device stack. The following subsections provide

Table 1 Status and challenges of the existing ARCs technologies

Types of ARCs	Deposition method	Material used	Gap and limitations in existing ARC technologies	Substrate	References
Planar	PVD	MgF_2	(1) MgF_2 films were deposited at 300 °C, a temperature that exceeds the thermal tolerance of perovskite solar cells, potentially causing degradation of the active layers (2) Refractive index mismatch arising from the selected substrate material can lead to suboptimal anti-reflective performance and reduced light coupling efficiency	BK-7, silica	47
Bilayer	Plasma etching & thermal evaporation	PMMA/CaF_2	(1) Plasma etching of the PMMA surface increases surface roughness, which may adversely affect the integrity and performance of subsequent device layers (2) CaF_2 deposition requires elevated temperatures that can cause thermal degradation of multiple layers within the device stack (3) Refractive index mismatch caused by the substrate selection can lead to inefficient light transmission and reduced overall device efficiency	PMMA substrate	48
Bilayer	Sol–gel & E-beam evaporation	MgF_2/SiO_2	(1) The substrate was heated to 300 °C during MgF_2 deposition and post-annealing after SiO_2 deposition; however, perovskite materials cannot tolerate such high temperatures without degradation (2) Refractive index mismatch arising from the choice of substrate can lead to decreased anti-reflective performance and reduced light transmission efficiency	Sodalime glass	49
Multilayer	E-beam & thermal evaporation	TiO_2/MgF_2	(1) The fabrication process requires substrate heating to 250 °C during deposition, followed by post-deposition annealing at 400 °C for 1 hour—conditions that exceed the thermal stability limits of perovskite solar cells and may cause device degradation (2) The ARC design involves 10 material layers, and prolonged exposure of PSCs to the high-vacuum environment necessary for such multilayer deposition can negatively impact device integrity and performance (3) Refractive index mismatch arising from the choice of substrate can reduce the anti-reflective effectiveness, leading to decreased light coupling and lower overall device efficiency	Bk-7	50
Porous	Dip coating	SiO_2	(1) Thermal annealing at 400 °C, which exceeds the thermal stability limits of perovskite solar cell materials and can cause device degradation (2) Coating both sides of the substrate, a process incompatible with PSC architectures due to the presence of a transparent conductive electrode on one side (3) Refractive index mismatch resulting from the substrate choice, which can lead to reduced anti-reflective performance and lower overall device efficiency	Sodalime glass	51
Porous	Sol–gel method	SiO_2	(1) SiO_2 coatings in this study were annealed at 450 °C for 1 hour to optimize film quality and porosity; however, perovskite materials are thermally sensitive and typically degrade at temperatures exceeding approximately 150 °C (2) The coatings were designed and evaluated on soda-lime glass substrates rather than directly on perovskite solar cell modules, meaning that their performance and durability may differ significantly when integrated into complete device stacks (3) Refractive index mismatches resulting from the choice of substrate can adversely affect the anti-reflective performance and overall optical efficiency of the coating	Soda-lime glass	52
Porous	Dip coating	TiO_2	(1) Annealing the deposited layer at 500 °C to achieve the desired porosity, a temperature that exceeds the thermal stability limits of many substrates used in perovskite solar cells (2) Hydrofluoric acid (HF) is employed to create porosity in the film; however, its use can cause damage to ITO-coated glass substrates, limiting its applicability in such configurations	Glass	53

Table 1 (*Contd.*)

Types of ARCs	Deposition method	Material used	Gap and limitations in existing ARC technologies	Substrate	References
Porous	Spin-coating	SiO_2	(1) Annealing of the deposited layer at 500 °C to obtain the desired porosity	Glass	39
Trabsferable	Vacuum filtration with PVA lamination	Cellulose fibres	(1) Cellulose is hygroscopic, which poses significant risks for perovskite materials due to moisture-induced degradation (2) A coating thickness of 50 μm is excessively thick for perovskite solar cell structures and may adversely affect the optical path length and overall device performance (3) The study focuses on applications in GaAs solar cells; however, differences in the refractive indices between GaAs and perovskite materials limit the direct applicability of these results to perovskite-based devices	Transparent paper (cellulose-based)	54
Porous	Dip coating	SiO_2/TiO_2	(1) Annealing the film at 450 °C is incompatible with perovskite materials and other layers within the device stack, as such high temperatures can cause degradation (2) Refractive index mismatch arising from the choice of substrate can adversely affect the optical performance and reduce the overall efficiency of the device	Soda lime glass	55

a comprehensive overview of each class, discussing key material systems, design strategies, fabrication methodologies, and the reported impact on PSC performance.

4.1. Planar and Graded-index ARCs

Planar ARCs are preferably fabricated using deposition techniques, including physical vapor deposition (PVD), sol–gel, dip coating, and slot die coating. With these methods, single-layer anti-reflection coatings (SL-ARCs) are the most commonly used for PSC device applications. As the refractive index of the coating material is crucial in determining its anti-reflective properties. A practical approach to producing such coatings is by evaporating low refractive index materials, such as lithium fluoride (LiF)[56] and magnesium fluoride (MgF_2),[57,58] using PVD techniques.

For example, as shown in Fig. 5, Paliwal *et al.*[59] applied a LiF ARC in a bifacial PSC device configuration. The LiF layer was thermally evaporated on both the bottom and the rear transparent electrode (TE) sides, resulting in a current density value change of approximately 1.72 mA cm^{-2} for 100 nm LiF on the glass ITO side and 75 nm LiF thicknesses on the rear electrode, respectively. Fig. 5(b) shows the 2D-contour plot obtained from optical Modeling for thickness optimization, while Fig. 5(d) and (e) represent the EQE and the J_{sc} value of the device with and without LiF ARC.

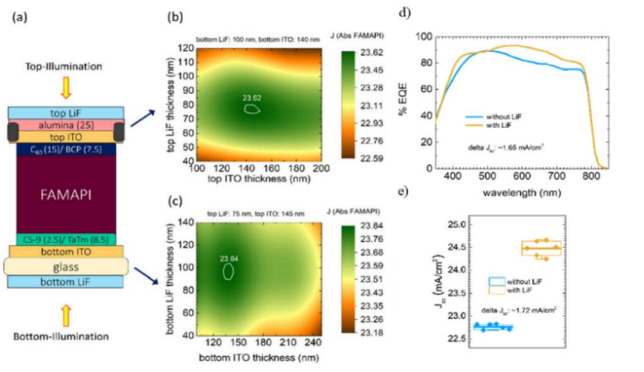

Fig. 5 (a) Bifacial PSC device architecture with ARC, (b) and (c) optical modeling graphs for optimization of bottom and top LiF layer, (d) EQE of the device with and without ARC, and (e) variation in the J_{sc} with LiF ARC. Reproduced from ref. 59 with permission from ACS Publications, copyright 2024.

While SL-ARC may not always be sufficient, its anti-reflective properties can be further enhanced by using a multiple-layer structure. When creating a multilayer ARC, it is essential to use materials with varying refractive indices (as shown in Fig. 1). Thus, the refractive index should follow an increasing sequence (*e.g.*, $n_1 < n_2 < n_3 < n_4 \ldots$), which forms a graded refractive index pattern.[60] In the case of PSCs, which typically use TCOs coated on glass as the bottom transparent electrodes, the refractive indices of these materials are around 2 (for TCOs) and 1.5 (for Glass), respectively. Thus, materials with ultra-low refractive indices are required to make an effective ARC. However, such materials are not commonly available. The lowest refractive index materials typically used are indeed MgF_2 and LiF, as previously discussed, which have refractive indices near 1.41 and 1.39, respectively.[56,57] Thus, developing a promising multilayer ARC presents significant challenges. One approach to overcoming this issue is to create materials with these ultra-low refractive index values. Kim *et al.*[61] in their study demonstrated an innovative way to control the intergranular voids between the grains of MgF_2, which resulted in solidified MgF_2 having an exceptionally low refractive index of approximately 1.04. They showed the formation of a multilayer ARC composed entirely of MgF_2 but with varying refractive indices layers. Fig. 6(a) illustrates the architecture adopted for the multilayer ARC, while Fig. 6(b) shows the change in the transmittance spectrum when the multilayer ARC was added. Moreover, they demonstrated that the developed ARC maintained its anti-reflecting properties at various incident light angles. Fig. 6(c) and (d) show the

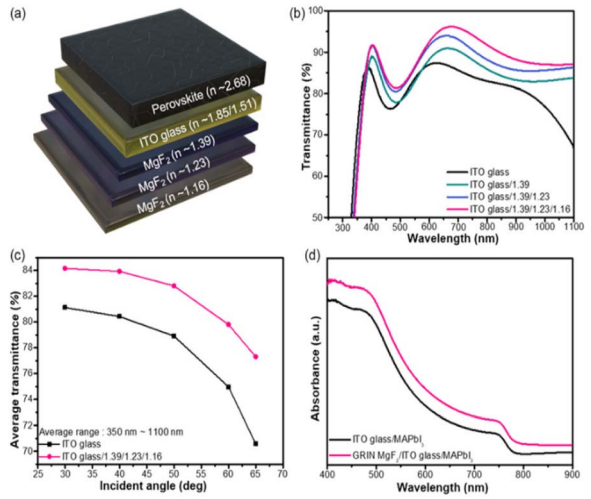

Fig. 6 (a) Gradient in the refractive indices values of the layers in the bilayer ARC, (b) refractive index of the used layer, (c) enhancement in average transmittance after the application of gradient ARC, (d) absorption spectra of the perovskite film with and without the gradient ARC. Reproduced from ref. 61 with permission from Wiley, copyright 2024.

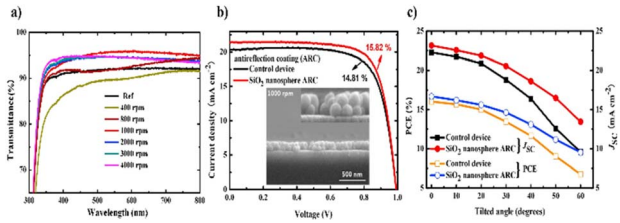

Fig. 7 (a) Transmittance spectra of ARC spin at different speed, (b) JV characteristics of the device with and without SiO_2 nanosphere ARC, (c) variation in the device J_{sc} and PCE with changing incident angle. Reproduced from ref. 36 with permission from Elsevier, copyright 2018.

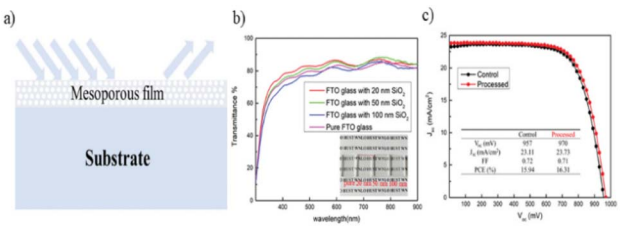

Fig. 8 (a) SiO_2 nanosphere mesoporous ARC, (b) transmittance spectra of FTO with SiO_2 having different particle size, (c) JV characteristics of the PSC with and without the optimized ARC Reproduced from ref. 62 with permission from Wiley, copyright 2022.

increase in the absorption spectrum of the perovskite photoactive layer after using the developed ARC. This approach of producing low-refractive-index MgF_2 offers a potential solution for developing other materials with similar properties. In comparison to other materials, such as polymers, MgF_2 is thermally and mechanically stable. However, the key challenge lies in precisely synthesizing the MgF_2 layer with ultralow refractive index values to achieve an effective multilayer ARC.

Thus, planar ARCs offer significant potential, especially for devices based on rigid substrates, due to their inherent mechanical robustness and compatibility with standard fabrication processes. Their optical performance can be further improved through multilayer configurations, which help broaden the antireflection range and reduce reflection over a wider spectrum. However, one of the key challenges associated with planar ARCs is the limited availability of low-refractive-index materials. This limitation becomes critical when aiming to optimize light manipulation at the air/substrate interface. For effective antireflection behaviour, it is essential to develop materials that combine ultra-low refractive indices with thermal and mechanical stability. Furthermore, these materials should ideally support simple, scalable deposition techniques to facilitate their integration into practical device architectures. Addressing this materials gap remains a crucial step toward realizing high-performance planar ARCs for PSCs.

4.2. Porous ARCs

Another effective type of ARC that enhances device current involves creating a porous structure. Nanoparticles can be utilized to create a porous layer, forming a pattern that traps light, thus improving light utilization efficiency and boosting overall device performance. For instance, Luo *et al.*[36] demonstrated the fabrication of silica nanospheres from an aged silica sol. The thickness of the SiO_2 nanospheres plays a crucial role in optimizing the ARC for a broad wavelength range. The SiO_2 nanospheres were deposited *via* spin coating method, and it was observed that varying the spin speed altered the microstructures of the nanospheres. This change in microstructure resulted in an increase in transmittance of approximately 3.8%, with a maximum transmittance of 96.1% at 550 nm. As a result, the photovoltaic current increased from 20.34 mA cm^{-2} to 21.39 mA cm^{-2}, while PCE rose from 14.81% to 15.82%.

Fig. 7(a) shows the transmittance spectra of a reference glass substrate and the glass substrate with SiO_2 nanospheres deposited at different spin speeds. As previously mentioned, spin speed affects the microstructure of the nanospheres, leading to observable changes in the transmittance spectra. Fig. 7(b) compares the JV characteristics of the fabricated device, demonstrating that the optimized SiO_2 nanosphere ARC led to an increase in the J_{sc} value. The inset figure is the cross-SEM image of the optimized ARC. Additionally, the optimized SiO_2 nanosphere ARC exhibited less angular dependence for light incident at various angles, as seen in Fig. 7(c). Since SiO_2 nanospheres were grown using a simple, inexpensive, and scalable process, this method is effective for large-area devices. However, it is essential to maintain precise control over the size of the nanospheres, as variations in size can impact the optical characteristics of the ARC.

Similarly, Wang *et al.*[62] developed a mesoporous SiO_2 film, as illustrated in Fig. 8(a), which resulted in a 2–4% increase in transmittance for FTO in the 350–800 nm wavelength range. The highest transmittance of the substrate reached 89%. They utilized a SiO_2 slurry composed of SiO_2 nanoparticles combined

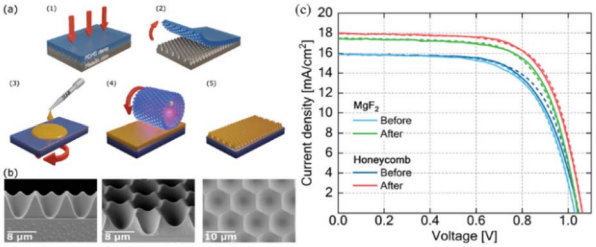

Fig. 9 (a) Schematic presentation of texturing of the surface, (b) surface morphology of the developed ARC, (c) JV characteristics of the PSC with planar MgF_2 and the honeycomb structure. Reproduced from ref. 17 with permission from Wiley, copyright 2023.

with an ethyl cellulose pore-forming agent. The ARC layer was then deposited using the scalable screen-printing method and annealed to form the porous SiO_2 ARC. Fig. 8(a) demonstrate the antireflecting phenomenon due to the presence of the mesoporous ARC. Fig. 8(b) shows a variation in FTO transmittance with different SiO_2 particle sizes achieved through this screen-printing technique. Fig. 8(c) shows the JV characteristics of the PSC with and without the optimized ARC.

Nanoparticle-based ARCs present a compelling route to address the fabrication challenges commonly associated with multilayer planar ARC configurations. Their inherently porous structure, due to the presence of air voids (with $n = 1$), enables more effective refractive index matching between air and the substrate, thus allowing the development of coatings with lower effective refractive indices. Furthermore, these coatings can be deposited using straightforward and scalable deposition techniques, such as spin coating, dip coating, or spray casting, which reduce process complexity and make them well-suited for large-area applications and flexible substrates. Optically, the incorporation of nanoparticles introduces additional light management mechanisms beyond conventional interference, including light scattering and near-field enhancement, which can enhance light coupling and increase absorption in the active layer. Moreover, nanoparticle-based ARCs offer the potential for surface functionalization, such as self-cleaning properties, which is a valuable feature in high-performance ARC applications.

Despite these advantages, a notable drawback of nanoparticle-based ARCs is their relatively poor mechanical robustness. Compared to dense, continuous planar films, nanoparticle coatings are more vulnerable to mechanical stress, abrasion, and environmental wear. Once damaged, their antireflective properties can degrade significantly, potentially compromising the overall device performance. This trade-off highlights an important consideration that while nanoparticle-based ARCs offer practical benefits in terms of fabrication and light management, their long-term stability under operational conditions remains a critical limitation. Addressing this issue, either through surface passivation, protective overlayers, or material engineering, will be essential for their broader implementation in durable perovskite solar cell technologies.

4.3. Textured and transferable ARCs

Textured ARCs are similar to porous ARCs, with the main difference being that, in the case of porous ARCs, one can lack control over the uniformity of the nanostructures over the film (size of the nanoparticles). In contrast, textured ARCs follow more specific patterns. These ARCs can aid in light trapping through multiple internal reflections due to their textured surface. Textured ARCs can be designed to create structures such as pyramidal, honeycomb, or other patterns of similar depth, giving them higher control over light utilization in the device. Textured ARCs can also be classified into two types: one where the device has a fixed, rigid textured layer, or one that allows the development of a transferable ARC. The following paragraph discusses both types of textured ARCs.

Krajewski *et al.*[17] in their work developed an ARC by texturizing the front surface of a device. They utilized SU-8 photoresist, which was spun on the opposite side of an ITO-coated glass substrate. After spinning, a replica of a honeycomb structure was created by nanoimprinting a textured PDMS stamp. To create the PDMS stamp, PDMS was dropped into a metallic mold (with a texture generally produced through lithography), which yielded the negative structure of the mold on the stamp. Fig. 9(a) and (b) show the full fabrication process for the honeycomb-textured ARC, while Fig. 9(c) shows a comparison of the JV characteristics of the PSC with honeycomb ARC and planar MgF_2 thin film, respectively. This approach successfully increased the device's J_{sc} from 15.9 mA cm^{-2} to 18 mA cm^{-2}, and its PCE from 11.1% to 13.1%.

Texturing the surface is a technique that is commonly employed in silicon solar cells and utilizes pyramid-shaped structures to enhance device performance by trapping light through the internal reflection phenomenon. Similarly, in this case, the texture and grain size of the film determine its

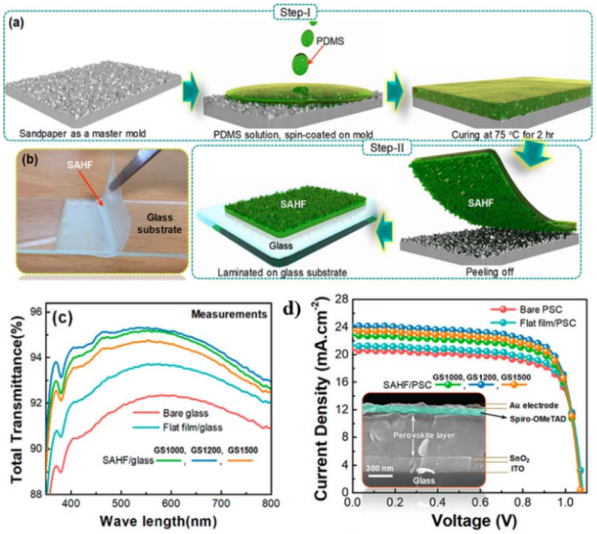

Fig. 10 (a) Schematic of the preparation of SAHF. (b) Transferable SAHF over the glass substrate, (c) transmittance spectra of the glass with SAHF of different grain sizes, and (d) JV characteristics of the PSC with and without SAHF. Reproduced from ref. 64 with permission from ACS Publishing, copyright 2019.

antireflecting properties. Another type of textured ARC includes the transferable ARCs, typically consisting of only a few microns-thick film, often made using polymers. These ARCs are particularly well-suited for flexible photovoltaic devices, as they maintain their bending properties unlike other ARCs discussed earlier. Dudem *et al.*[63] demonstrated the creation of flexible ARCs using sandpaper as a mold. They spin-coated a PDMS solution onto sandpaper with various grain sizes, which served as the master mold. The coated films were then cured at 75 °C for 2 hours and peeled off, resulting in a haze film. When these films were used as ARCs, the performance of the PSCs significantly improved. Without the ARC, the devices exhibited a J_{sc} of 20.88 mA cm^{-2} and a PCE of 17.07%. However, with the developed ARC, the J_{sc} increased to 23.73 mA cm^{-2}, and the PCE improved to 20.34%. Fig. 10a and b illustrate the method for casting the transferable ARC, while Fig. 10(c) shows the transmittance spectra of the glass substrate with and without the developed ARC, depending on the size of the sandpaper master mold. Fig. 10(d) presents the *J–V* curves for devices with ARCs based on different grain sizes.

While the use of sandpaper as the master mold for transferable ARCs may seem like an unideal approach, another alternative involves designing a patterned master mold to create more refined ARCs. A similar method was presented by Choi *et al.*,[64] where they used a silicon master to create a moth-eye structure through lithographic techniques. The size of the moth-eye structure directly impacted on the ARC's performance. They then deposited the PFPE polymer and pressed it using a PET film. After partial curing and solvent-assisted separation, a sticker-like ultra-thin perfluoropolyether (PFPE) (SUPA) antireflection film was formed. Fig. 11(a) demonstrates the process of making the SUPA, while Fig. 11(b) shows the atomic force microscopy (AFM) image of the moth-eye structure SUPA ARC, Fig. 11(c) shows the transmittance spectrum of the FTO substrate with and without SUPA, whereas Fig. 11(d) shows the external quantum efficiency of the photovoltaic device with and without the SUPA. They showed that the PFPE material alone increases light transmission efficiency (LTE) by only 4%.

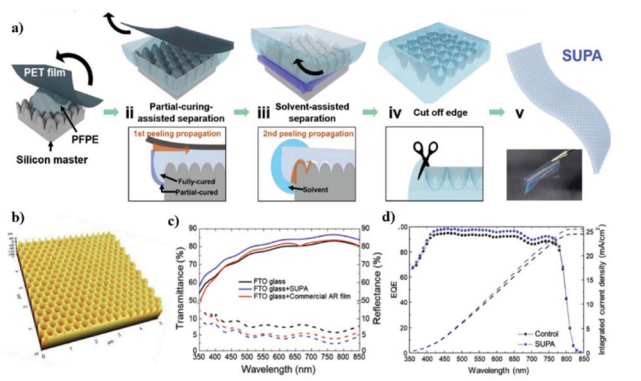

Fig. 11 (a) Schematic of the preparation of SUPA ARC, (b) AFM of the SUPA ARC having moth-eye structure, (c) transmittance spectra of the FTO glass with SUPA, and (d) EQE of the PSC with and without SUPA. Reproduced from ref. 64 with permission from Wiley, copyright 2022.

However, incorporating the moth-eye structure within the same material boosts the LTE by 8% (doubles the value w/*o* the moth-eye structure). The corresponding *J–V* curve reveals that the J_{sc} of the device rises from 24.47 mA cm^{-2} to 25.53 mA cm^{-2}, leading to a PCE increase from 23.10% to 24.43%.

Moreover, when it comes to flexible or bendable PSCs, traditional planar or porous ARCs may not be the most suitable options. Planar ARCs often lack conformability, while porous ARCs, despite their low refractive index due to the inclusion of air voids, suffer from poor thermal and mechanical robustness. As discussed earlier, the demand for ARCs that provide both a low refractive index for effective antireflection and structural resilience becomes even more critical in flexible PSCs. There is a clear need for coatings that can maintain performance under bending, stretching, or folding, while also enhancing light trapping and transmission.

In this context, textured ARCs are a highly promising solution. As shown in Fig. 9–11, these ARCs can be realized either by directly texturing the substrate surface or by fabricating transferable, sticker-like textured ARCs that can be applied to flexible devices. Such textured surfaces create micro- or nano-scale patterns that enhance light transmission by promoting light trapping and confinement through scattering and refraction mechanisms. This makes them highly effective for improving optical efficiency in a wide range of applications.

Although textured ARCs show strong performance across various sectors, a key challenge lies in precisely controlling the surface texture, as the antireflective behaviour depends heavily on the texture geometry, periodicity, and feature size. Achieving optimal textures typically requires advanced fabrication techniques, such as lithography, which can add complexity and cost to the process. Nevertheless, with proper control and design, textured ARCs offer an excellent balance of optical performance, mechanical durability, and flexibility, making them ideal candidates for ARCs for next-generation PSCs.

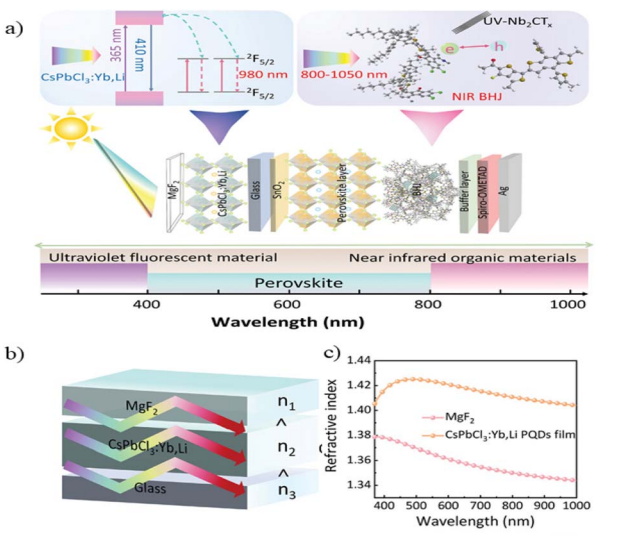

Fig. 12 (a) Schematic of the complete device architecture with the down-conversion layer, (b) gradient in the refractive index values of the layers in the bilayer ARC, (c) refractive index of the used layer. Reproduced from ref. 69 with permission from Wiley, copyright 2024.

4.4. Down-conversion ARCs

Down-conversion materials play a dual role in improving device performance, while also addressing photo-induced degradation issues in PSCs. In fact, down-conversion-based ARCs can aid in converting ultraviolet (UV) light to visible light, since such types of ARCs can absorb near-UV light and re-emit it as visible light, increasing usable photon flux by the perovskite material. Furthermore, as PSCs are vulnerable to UV radiation, which can degrade the perovskite layer by breaking chemical bonds and promoting ion migration, reducing device performance and lifespan,[65] the presence of down-conversion materials not only enhances light absorption but also provides UV shielding for the device.

Generally, the down-conversion-based ARC is achieved by incorporating photoluminescent materials such as lanthanide-doped phosphors, QDs, or organic dyes that absorb high-energy photons and emit longer wavelengths matching the perovskite absorption spectrum.[66,67] However, fabricating these coatings is challenging due to the need for precise integration of luminescent materials into a stable matrix, ensuring uniform dispersion, high quantum efficiency, and long-term stability under solar exposure. The synthesis often involves complex chemical processes, high-temperature treatments, and strict control over particle size and surface chemistry.[68] Addressing these challenges is essential for developing efficient and durable down-conversion ARCs for PSCs.

For instance, Shi *et al.*[69] designed a quantum-cutting down-converter that enhanced the utilization of UV light. Additionally, the deposition of a MgF_2 anti-reflection coating (ARC) over the quantum-cutting layer formed a waveguide-structured ARC, further improving light utilization due to the gradient in refractive index values. Fig. 12(a) illustrates the down-conversion mechanism in PSCs by incorporating a bilayer ARC consisting of MgF_2 and $CsPbCl_3$: Yb, Li. The sequence of increasing refractive indices (depicted in Fig. 12(b)) across the layers created a gradient in refractive index values, which enhanced device performance. Fig. 12(c) shows the refractive index of the layers used in the bilayer ARC. When integrated into the device architecture, the presence of the ARC increased the J_{sc} from 25.56 mA cm^{-2} to 26.65 mA cm^{-2}, and the PCE from 23.07% to 24.3%.

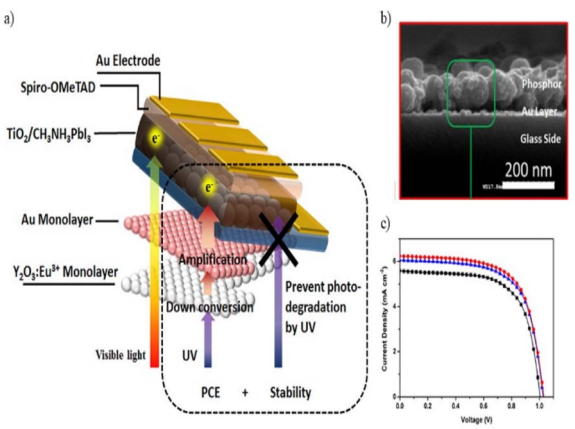

Fig. 13 (a) Schematic illustration of the dual functioning of the down-conversion film for PSC, (b) cross-SEM image of the dual film, (c) JV characteristics with and without the downconverter film (black for ref PSC, blue with phosphor monolayer, and blue for phosphor on Au monolayer). Reproduced from ref. 70 with permission from Springer Nature, copyright 2017.

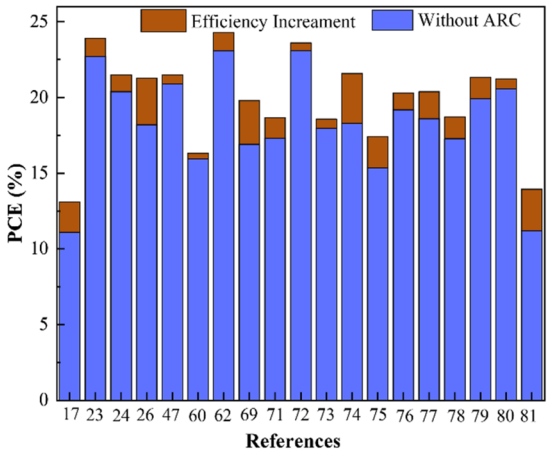

Fig. 14 Efficiency enhancement in PSCs after incorporating various ARCs existing in the literature.

Similarly, Kim *et al.*[70] developed a downconverter film consisting of Y_2O_3: Eu^{3+} that increased the quantum yield to over 80% in the visible light region. Furthermore, the incorporation of gold (Au) nanoparticles amplified the converted light by up to 170%. Fig. 13(a) illustrates the down-conversion process, which helps boost the PCE and prevent photodegradation. The cross-sectional SEM image in Fig. 13(a) shows the phosphor monolayer on the gold monolayer. Fig. 13(b) presents the photoluminescence emission spectrum for the phosphor monolayer (shown in black) and the dual-layer ARC (shown in red).

To sum up, having discussed the various types of ARCs explored for PSCs, Fig. 14 provides a visual comparison of different ARCs applied in PSCs, encompassing all previously discussed ARC configurations. The figure illustrates the resulting improvements in PCE for each type of ARC, underscoring the critical role ARCs play in optimizing light management and enhancing the overall performance of PSCs.

Furthermore, Table 2 presents a comparative overview of the ARC strategies for PSCs (illustrated in Fig. 14), highlighting the fabrication methods used to prepare the ARCs, the types of substrates employed, and the performance of these coatings under standard AM1.5 illumination. In addition, the table summarizes the reported improvements in device performance, along with key information on the stability, durability, and distinguishing functional features of each ARC, enabling a clearer comparison of different coating approaches.

5. Fabrication techniques for ARCs

5.1. Sol–gel based techniques

The Sol–gel technique is highly favoured for its ease of integration and versatility, involving the use of material precursors

Table 2 Comparison of different types of ARCs for PSCs based on various parameters

ARC type	Fabrication method	Substrate	J_{sc} gain	Stability & key features	References
Roller nanoimprinted honeycomb texture ARC	Roller nanoimprint lithography (R2R-compatible)	Rigid glass	18%	Broadband reflection suppression through periodic honeycomb nano-texture; scalable large-area fabrication; improved light harvesting and mechanical durability suitable for industrial processing	17
Silica nanosphere ARC	Spin-coating	Rigid	4%	Light scattering minimized, enhanced transmittance, moderate durability	23
Bilayer broadband dielectric ARC	Multilayer coating	Rigid	5.5%	Stable multilayer design, broadband ARC	24
Durable sol–gel self-cleaning ARC	Sol–gel process	Rigid	6%	Strong abrasion resistance, self-cleaning	26
Amorphous MgF_2 ARC	Thin-film deposition	Rigid	16.9%	Improved stability, simple MgF_2 ARC	47
Graded-index mesoporous Al_2O_3	Mesoporous coating	Rigid	3%	Good long-term stability, graded index design	60
Printable mesoporous SiO_2	Printing	Rigid	6%	Scalable fabrication, mechanical stability	62
MXene-modified waveguide & down-converter	Solution + waveguide structuring	Rigid	5%	Broad spectral coverage, enhanced NIR absorption, stability improved *via* MXene integration	69
$NaYF_4$:Eu^{3+} nanophosphor down-conversion layer	Solution processing	Rigid	17%	Converts UV to visible, improved J_{sc}, moderate stability	71
Photocurable fluoropolymer coating	Spin-coating	Rigid	7%	Self-cleaning, hydrophobic, improved stability against moisture and oxygen	72
Down-shifting quantum dot coating	Spin-coating	Rigid	2%	Moisture-assisted film growth, enhanced light management, stability improved	73
Nitrogen-doped graphene quantum dots	Spin-coating	Rigid	3%	High photoluminescence, down-conversion, improved J_{sc} and stability	74
Demixed blended polymer textured interface	Spin-coating	Rigid	18%	Coordinated optical matching, reduced reflection, improved inverted PSC performance	75
Mesoporous & hollow silica ARC	Sol–gel	Rigid	14%	High stability, enhanced transmittance, moisture-resistant, self-cleaning	76
Plasma-polymerized fluorocarbon ARC	Plasma polymerization	Flexible	6%	Flexible, high optical transmittance, hydrophobic, improved operational stability	77
Water-based SiO_2 ARC	Sol–gel	Rigid	10%	High optical transmittance, self-cleaning, eco-friendly fabrication	78
MgF_2 thin-film ARC	Thermal evaporation	Rigid	8%	Low optical loss, stable under standard conditions, simple fabrication	79
$CH_3NH_3PbI_3$ planar perovskite ARC + self-cleaning	Spin-coating	Rigid	3%	Self-cleaning, hydrophobic, enhanced J_{sc} and device stability	80
Anti-reflection protection layer	Spin-coating	Rigid	3%	Water-repellent, stable under ambient fabrication, enhanced optical transmission	81

Table 3 Techno-economic comparison of various ARCs fabrication techniques

Parameters	Sol–gel	PVD	Nanostructuring/lithography
Material cost	Low	High	High
Process complexity	Low	Moderate to high	High
Energy consumption	Low	High	High to very high depending on lithography method
Scalability	Large-area compatible	Moderate scalability (upto large wafer size)	Low large -scale scalability
Main advantages	Simple processing	Precise thickness control, high film quality	Higher design flexibility, superior optical performance
Limitations	Limited stability and thin film uniformity	High equipment cost, limited throughput	Very high fabrication cost, not compatible for large area production

in compatible solvents, which allows for the self-assembly of nanostructured surfaces through a "bottom-up" approach. Common sol–gel-based deposition methods for ARCs include dip coating, spin coating, and spray coating. In dip coating, the substrate is dipped into the solution and then withdrawn at a controlled rate, determining the coating thickness.[82] Spin coating, which is another widely used sol–gel technique, is also employed to form thin films on flat surfaces. The centripetal force during spinning spreads the material evenly, with the film thickness controlled by adjusting the spinning speed or material viscosity.[37,82] While spin coating is simple and efficient, it is not ideal for large-area applications. On the other hand, the dip coating technique is viable for larger surfaces, poses challenges in handling large substrates and ensuring consistent coating thickness. Without careful control during the dipping process, an uneven coating can occur, which can negatively impact the optical properties of the film. Thus, spray coating is another practical, simple, and scalable method for ARC deposition. In spray coating, factors such as nozzle-to-substrate distance, air pressure, droplet size, solution concentration, flow rate, and viscosity must be carefully controlled, as each factor influences the final film thickness. While sol–gel films are easy to fabricate, material waste during deposition and residual solvent can affect the ARC properties. Additionally, optimizing parameters for reproducible film thickness is crucial, as even minor changes in precursor solution composition or deposition conditions can impact the film thickness and optical properties. For this reason, Physical Vapor Deposition (PVD) is a commonly used technique for ARC fabrication.

5.2. Physical vapor deposition techniques

PVD techniques are among the most commonly used methods due to their ability to produce films with consistent qualities. Thermal evaporation is typically used for depositing ARCs. This process involves the condensation of vaporized material onto the substrate.[42] Low refractive index materials like MgF_2 and LiF are commonly used in this method, serving as effective ARCs for PSCs. However, the question arises: how can this technique be further optimized for enhancing anti-reflective properties? The answer lies in an advanced technique called Glancing Angle Deposition (GLAD). In this method, the vapor flux is directed at a substrate rotated at a specific angle. One key advantage of GLAD is that as the material is deposited, the density of the deposited material decreases gradually. This results in an increased porosity of the film due to the atomic shadowing effect. Moreover, GLAD offers superior control over the morphology of the resulting nanostructure compared to the sol–gel method. Since GLAD creates a porous, thin film, it also influences the refractive index of the material. For instance, a material deposited on a flat surface exhibits a different refractive index than one deposited on a tilted substrate due to the porosity of the thin film.

5.3. Lithography and patterning the substrates

The above-mentioned are the most commonly used techniques for fabricating ARCs for PSCs. However, another less conventional method, though reported in the literature, is lithography-based ARCs. This process involves patterning the surface of a substrate to create nanoscale features. It can be used to create patterns on the opposite side of TCO-coated glass, which can enhance light utilization through the phenomenon of internal reflection. Additionally, this technique is often employed for template-assisted micro-replication in ARC fabrication.[64]

In this process, a specific pattern is formed on a mold, and then a polymer material is cast into the mold. Once the polymer material is removed, it retains the pattern on one side and can be used as a textured ARC; the examples for this type of ARC have been discussed in detail in Section 4.3.

Hence, this section outlined key fabrication techniques for ARCs specifically in the context of PSCs, focusing on their effectiveness, scalability, and compatibility with PSC architectures. Sol–gel-based methods offer a low-cost, solution-processable route to form ARC layers with tuneable thickness, making them suitable for lab-scale PSCs. However, challenges such as film uniformity, material waste, and limited scalability must be addressed for industrial applications. PVD, including advanced methods like GLAD, enables the formation of uniform, porous ARC layers with finely tuned refractive indices that significantly enhance light management in PSCs. Despite its precision, PVD involves higher complexity and cost. Lithography and substrate patterning techniques, while less commonly used, present promising opportunities for creating nanostructured ARC surfaces that improve light trapping *via* internal reflection. Although more complex, these methods can

be particularly effective for high-performance PSCs where maximizing optical absorption is critical. Selecting the appropriate ARC fabrication technique for PSCs thus depends on balancing optical performance, processing complexity, and scalability. From a techno-economic perspective, different fabrication methods for ARCs involve distinct trade-offs in material cost, process complexity, energy consumption, and scalability. Sol–gel based fabrication techniques usually offer the lowest material and equipment cost and the highest potential for large-area production due to its compatibility with low-temperature processing and roll-to-roll manufacturing, making them particularly suitable for commercial applications. In contrast, PVD techniques provide precise control over thin films, but at the same time require high capital investment, greater energy consumption, and provides moderate scalability, restricting their suitability for very large area coating. While Nano structuring, and lithography techniques gives advance control of thin film fabrication and resulting properties. However, their complex multi-step processing and dependence on specialized equipment's result in higher production costs and does not suits for large scale deployment. Furthermore, depending on the type of lithography method the energy consumption can be very high due to high-power sources. Overall, each fabrication technique has its own unique advantages, but the trade-offs between cost, complexity, energy and scalability must be carefully considered to identify the most industrially viable ARC fabrication method. Table 3 given below represents a systematic comparison of these techniques in terms of material cost, process complexity, energy consumption, and scalability potential.

6. Key considerations in designing an ARC for PSCs

When a solar cell is deployed in any external environment, such as on sunroofs, cars, houses, or fields, it is crucial to maintain its performance as demonstrated in the laboratory. However, achieving consistent performance in a real-world scenario is challenging.[31,83] This section will discuss the key issues and strategies for mitigating power loss using ARCs for PSCs.

6.1. Anti-soiling properties of ARCs

Under the operational conditions, the ARCs are exposed to external factors such as sunlight, humidity, dust, dirt, and organic matter, soiling losses become a significant concern. These soiling issues arise not only from the accumulation of dirt on the ARC but can also be caused by various other factors. Fig. 15 provides an overview of different types of soiling with exemplary images.[83–86] Such soiling can lead to light attenuation, ultimately reducing the output power of the solar cell.

Maintenance of solar cells can be carried out manually, semi-automatically, or with fully automatic machinery. However, if the solar plant covers a large area or if the solar cells are used in building-integrated photovoltaics (BIPV) or aerospace applications, maintenance becomes a bit challenging. Therefore, in addition to these maintenance techniques, assessing the anti-

Fig. 15 (a–f) Overview of different soiling types with exemplary photographs of the soiling of the PV panels. Reproduced from ref. 83–86 with permission.

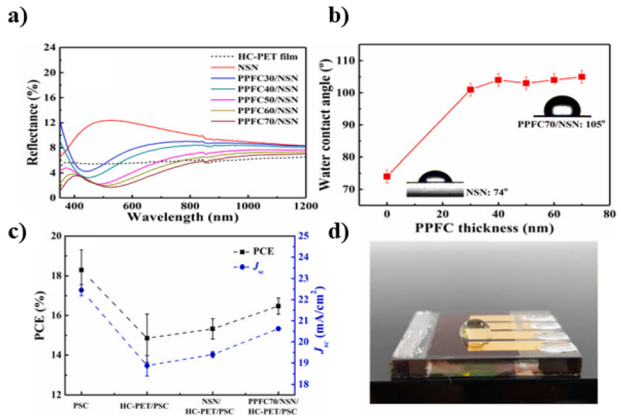

Fig. 16 (a) Change in the reflectance with different thicknesses of PPFC, (b) water contact angle at different PPFC thickness, (c) variation in J_{sc} and PCE with the optimized ARC, (d) real-time image of the device. Reproduced from ref. 87 with permission from Elsevier, copyright 2019.

soiling properties of any ARC is crucial for ensuring its long-term effectiveness. Kim *et al.*[87] in their study developed a multilayer ARC consisting of $Nb_2O_5/SiO_2/Nb_2O_5$ and introduced a capping layer of plasma-polymerized fluorocarbon (PPFC) to create a water-repellent surface. This modification reduced reflectance to 1.71% in the visible spectrum and produced a hydrophobic surface with a contact angle greater than 100°. The improved film enhanced photocurrent collection when applied to PSCs. Fig. 16(a) shows the reflectance of the NSN ARC with various PPFC layer thicknesses, while Fig. 16(b) illustrates that a 70 nm PPFC layer results in a contact angle exceeding 100°. Fig. 16(c) shows changes in the device PCE and J_{sc}, and Fig. 16(d) presents a real-time image of a water droplet on the fabricated device. The results demonstrated that incorporating PPFC into the ARC not only reduces soiling but also makes the surface self-cleaning, an essential feature for an effective ARC.

Similarly, Tavakoli *et al.*,[6] in their paper, developed a textured ARC with self-cleaning properties. The developed

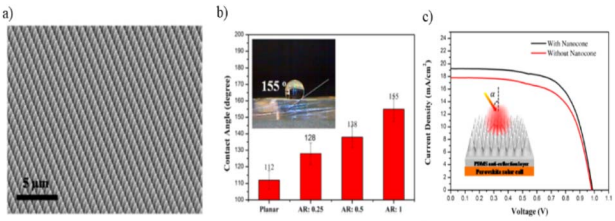

Fig. 17 (a) SEM images of the PDMS nano cones, (b) water contact angle of deionized water on PDMS layer with different aspect ratio, (c) JV characteristics of the device with and without the PDMS nano cone film. Reproduced from ref. 6 with permission from ACS Publications, copyright 2015.

textured ARC features nano cones that enhance light management within the device, increasing the device J_{sc} from 17 mA cm^{-2} to 19.1 mA cm^{-2}. Additionally, this ARC exhibited water-repelling properties with a contact angle of up to 155°. Such ARCs are beneficial for maintaining the cleanliness of solar cells. Fig. 17(a) shows the SEM cross-sectional image of the nano cone ARC, while Fig. 17(b) presents the water contact angle measurement. Fig. 17(c) display the J-V characteristics of the device with and without the ARC. Such ARC can increase the charge carrier generation rate, demonstrating the increase in photocurrent generation after incorporating the ARC, as seen by the JV curve.

6.2. Infra-red reflecting coatings

Continuous exposure of solar cells to sunlight can also lead to an increase in their temperature, which poses a significant challenge for consistent device performance. Elevated temperatures result in a reduction in efficiency and accelerate degradation processes, ultimately shortening the device lifespan. Therefore, when designing an ARC, it is essential to address this issue. The ARC must not only provide effective anti-reflection properties but also help minimize heating by reflecting the bandgap radiation responsible for temperature rise. Maniyara *et al.*[88] made notable progress in this area by designing an anti-reflective transparent conductor with minimal optical loss, achieving over 98% transmission in the visible spectrum. Likewise, Perrakis *et al.*[89] developed an infrared-reflective transparent electrode that also exhibited minimal optical losses. Their design showed over 91% transmission in the visible range and about 70% reflection in the infrared range. This innovation significantly reduced the device heat load by 128.9 W m^{-2}. In their study, one device featured the conventional FTO transparent electrode, while another used the infrared-reflective transparent electrode. Fig. 18(a) and b show the operating temperature of the cell under various environmental conditions, including wind speed, ambient temperature, and relative humidity. The presence of such IR reflecting ARC resulted into an average decrease of 6° in device operating temperature, which can significantly enhance the operational stability of the PSC. Further, Fig. 18(d) shows the JV characteristics revealing that the optimized transparent electrode increased the J_{sc} from 23.47 mA cm^{-2} to 24.60 mA cm^{-2} and Fig. 18(e) shows the reflectivity of the designed transparent electrode, which contributed to a reduction in the thermal load from 501.1 W m^{-2} to 372.2 W m^{-2}.

6.3. Durability of ARCs

In addition to their anti-soiling and infrared-reflecting properties, one of the most critical characteristics of a good ARC is its mechanical durability. Over time, ARCs can degrade due to various factors. Physical damage to the ARC surface can occur from environmental conditions such as hailstorms, bird scratches, and temperature fluctuations. Additionally, the performance of the coating can deteriorate due to certain cleaning practices, especially in areas prone to sandstorms and other harsh weather conditions. Regular cleaning of ARCs, while necessary to maintain their function, can lead to abrasion damage. Fig. 19(a), presents a SEM image of an ARC coating that has been damaged by abrasion.[28] Abrasion damage can occur in two primary ways. First, when a uniform amount of material is removed from the entire ARC surface, the coating thickness is reduced, which in turn diminishes its anti-reflective properties. Thinning of the ARC can also result from exposure to acidic

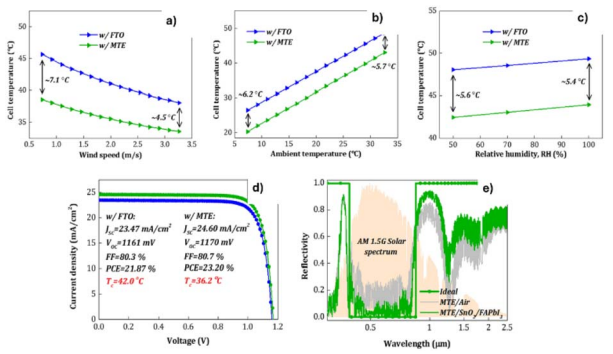

Fig. 18 (a)–(c) Variation in the operating temperature of the device under various environmental conditions after the application of IR reflecting coating. (d) JV characteristics of the PSC, (e) Reflectivity after the application of the IR reflecting coating. Reproduced from ref. 89 with permission from Springer Nature, copyright 2024.

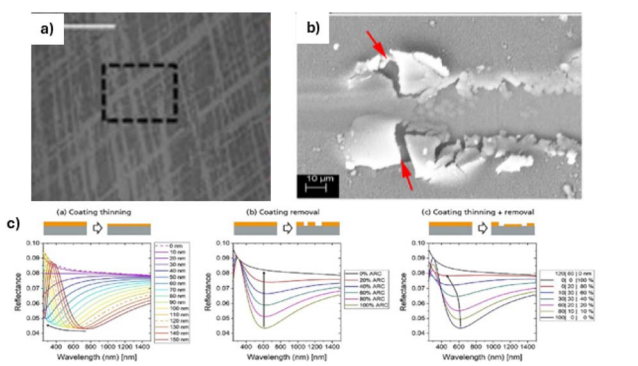

Fig. 19 (a) ARC damage due to abrasion,[28] (b) ARC damage due to material removal,[42] (c) types of ARC damage (i) thinning process, (ii) coating removal, (iii) thinning and coating removal simultaneously.[34] Reproduced from ref. 28, 34 and 42.

Table 4 Stability and durability strategies for ARCs under environmental stress

Targeted functionality	Environmental conditions tested	Trade-offs	Optimization strategies	References
ARC on PV cover glass	Damp heat, abrasion (scratch/abrasion tests)	Hygroscopic sol–gel ARC degrades in humid climates	Strong adhesion, hard coat, but limited humidity durability	90
Anti-soiling + ARC	Desert soiling, UV, abrasion	Soiling reduces transmittance; dusty environments	Combining ASC & ARC materials, field/accelerated testing (soiling & cleaning)	91
ARC performance in a harsh climate	Dust/soiling, abrasion (1500 cycles)	Long-term cleaning abrasion can degrade transmittance	High abrasion resistance with minimal loss (~2.6% after 1500 cycles)	92
ARC + superhydrophobic/ self-cleaning	Outdoor exposure, mechanical tests	Roughness *vs.* optical transparency	Double-layer structure with embedded silica for adhesion/mechanical stability	93
ARC + self-cleaning composite	UV irradiation, outdoor conditions	Balancing AR *vs.* hydrophobic functions	Low-temp composite (MMA@MQ), scalable coating, enhanced robustness	94
Dense multilayer ARC	Abrasion, cleaning cycles	Porous ARCs easily damaged	Dense multilayer/silica ARCs for enhanced durability	91
ARC + negative temperature tolerance	Temperature durability, mechanical abrasion, and hydrophobicity effects	Trade-offs between transparency & durability	Multilayer designs, optimal surface chemistries	42
ARC + self-cleaning	General environment (UV, dust)	Limited long-term testing previously	Highlights combined AR/ Self-cleaning synthesis methods	31
ARC + ASC abrasion	Mechanical abrasion, cleaning cycles	ARC wear from cleaning	Reinforced coatings, abrasion testing protocols	91
ARC + photocatalytic self-cleaning	UV irradiation (photocatalysis)	Photocatalytic layer absorption risk	Sol–gel SiO_2 optimized for AR + self-cleaning	95

environments, making air pollution a significant factor in the degradation process, sometimes overshadowing other environmental stressors. The second form of damage occurs when a section of the ARC is entirely removed, leading to more extensive damage, as shown in Fig. 19(b).[42] Fig. 19(c) shows the categories of the types of ARC removal. When the ARC is simply thinned, only a minimal change in reflectance is observed. In contrast, when a significant portion of the material is removed from the surface, the reflectance is more noticeably affected. The most severe degradation occurs when both thinning and the removal of sections of the ARC happen simultaneously, which results in a combined effect that drastically impacts reflectance.[34]

As the durability of ARCs is a critical factor for their effective performance, recent literature has examined their behavior under environmental stresses such as damp heat, UV irradiation, mechanical abrasion, and soiling, highlighting how these challenges can be mitigated through various strategies. The Table 4 below summarizes these recent advances.

Thus, in addition to strong antireflective performance, an ideal ARC should also possess anti-soiling properties, preventing the accumulation of dust, water droplets, and environmental contaminants on the surface. This ensures consistent optical performance over time and reduces the need for frequent maintenance. Moreover, the ARC should exhibit infrared (IR) reflecting capabilities, which help to minimize heat buildup by reflecting unwanted IR radiation, thereby maintaining the device operational temperature within an optimal range. This thermal regulation is crucial for improving the long-term stability and efficiency of PSCs. Furthermore, the coating must demonstrate high mechanical durability, ensuring it remains intact and effective even under physical cleaning, environmental wear, or repeated handling.

It should resist abrasion, peeling, or degradation during routine maintenance processes. Collectively, these multifunctional properties, including anti-reflective, anti-soiling, IR-reflective, and mechanically robust, are essential for developing ARCs that can perform reliably in real-world outdoor and industrial environments. Now, although multifunctional ARCs provide additional benefits, including self-cleaning behavior, thermal regulation, and enhanced durability, the integration of multiple functionalities may introduce trade-offs with optical performance. For example, micro- and nanostructures designed to impart superhydrophobicity and self-cleaning characteristics often increase surface roughness and light scattering, which can reduce optical transmittance. Similarly, the incorporation of infrared reflecting materials or mechanically reinforced layers may alter refractive index matching and optical interference conditions, potentially compromising ARC performance. Recent studies indicate that these trade-offs can be effectively minimized through rational material and structural design. Strategies such as ordered nano structuring with precisely

Table 5 Trade-offs and optimization strategy for targeted functionalities of ARCs existing in the literature

Targeted functionalities	Reported trade-offs	Optimization/coordination strategy	References
ARC, durability, outdoor stability	Porous ARC layers vulnerable to abrasion and contamination	Multilayer designs combining dense base layers with functional top layers	96
ARC + self-cleaning	Surface roughness for self-cleaning increases light scattering	Controlled nano-roughness and refractive-index grading	31
Transparency, self-cleaning, durability	Hydrophobic textures reduce transparency at high roughness	Balance between nanoscale texture size and optical wavelength	17
ARC + super hydrophobicity	Superhydrophobic microstructures induce optical losses	Use of sub-wavelength nanostructures to suppress scattering	97
ARC, super hydrophobicity, robustness	Mechanical wear degrades surface texture	Composite nanofiber–silica systems to enhance mechanical strength	98
ARC, weather resistance, self-cleaning	Hydrophobic chemistry can alter refractive index matching	Sol–gel tuning of porosity and surface functionalization	99
ARC, super hydrophobicity, durability	Eco-friendly materials may reduce hydrophobic efficiency	Bilayer design: AR base layer + hydrophobic top layer	100
ARC, self-cleaning, mechanical stability	Biomimetic textures risk excessive roughness	Hierarchical structures with nanoscale optical control	101
ARC, super hydrophobicity	High-aspect-ratio structures scatter light	Optimized aspect ratio and fluoropolymer infiltration	102
ARC, self-cleaning	Balancing optical transmittance, hydrophobicity, and mechanical robustness	Composite MMA@MQ coating with controlled layer thickness and low-temperature scalable deposition (spin-coating, dip-coating) to maximize ARC and self-cleaning while ensuring durability	94

controlled feature sizes, hybrid composite coatings, and optimized multilayer architectures have proven successful in balancing functionality and optical efficiency. Furthermore, the application of optical Modeling and surface energy engineering can facilitate the simultaneous optimization of transparency, durability, and environmental resistance. These integrated design approaches provide a practical pathway for developing multifunctional ARCs with minimal compromise in optical efficiency. Table 5 summarizes recent literature demonstrating how these properties can be coordinated and optimized concurrently.

Additionally, as discussed earlier, the development of a high-performance ARC involves numerous interdependent factors. Thus, rather than relying solely on material selection, it is recommended to employ simulation and Modeling tools to guide the design process before experimental trials. This approach reduces trial-and-error chances and enhances the likelihood of achieving an optimal ARC for PSCs without material and time wastage. The following section explores the role of simulations in advancing ARC development for PSCs.

7. Role of optical modeling and machine learning in designing optimal ARCs for PSCs

Modeling plays a key role in designing optimal ARCs, saving both materials and time. Before conducting real-time experiments, an effective approach to designing an optimal ARC is to predetermine the ideal thickness values, which can be guided through Modeling techniques. One widely used method for this is optical Modeling, typically based on the transfer matrix method.[103,104] Optical Modeling is a well-known and widely opted technique used for the optimization of multilayer structures, including ARCs,[105] photonic crystals,[5,106] transparent electrodes,[107,108] and photonic devices including solar cells.[109–111]

To perform this Modeling, optical constants data of each layer is required as the input parameter, whereas to get reliable results from Modeling it is crucial to adopt accurate optical constant data for each thin film, as a slight variation in the measurement of the optical constant data can led to the changes in the optimising results for thin film structures (as even small deviations can significantly affect the optical properties.[112] Therefore, the Modeling process should closely align with the experimental setup, considering all layers in the same manner. This approach also enables the exploration of different configurations and the selection of materials with the optimal refractive indices for maximum performance. Thus, in addition to optimizing thickness, simulations also assist in choosing materials with the ideal refractive index for maximizing the device efficiency. To model this behaviour, the Fresnel Equation is commonly used, as it provides a fundamental mathematical concept to calculate the optical characteristics (transmittance, reflectance, and absorption) at a particular interface.[104] As previously discussed in the introduction, Fig. 1(a) and (b) illustrate how light waves propagate through a single-layer and a multilayer ARC on a substrate, respectively.

ARCs can be single, bilayer, or multilayer, depending on their effectiveness. For a single-layer ARC as shown in Fig. 1(a),

in the introduction, the two reflected rays, R1 and R2, must interfere destructively to minimize reflection. To achieve this, the optimal thickness for such a single-layer ARC corresponds to a quarter-wavelength of the incident light at the coating central wavelength. Thus, for the single-layer ARC to perform optimally, the material must satisfy a specific relationship between its refractive index and the wavelength of incident light. Specifically, if n_{arc} represents the refractive index of the ARC, and n_a and n_s are the refractive indices of the media on either side of the coating (air and substrate, respectively), the refractive index of the ARC should ideally follow the relation:

$$n_{arc} = \sqrt{n_a n_s} \quad (1)$$

As Fresnel's Equation depends on the polarization of light (*s* and *p* polarization), thus, the equation expressing the phase difference is given by:

$$\delta = 2\pi n d \cos\theta/\lambda \quad (2)$$

For a normal incidence case (where $\theta = 0$), the reflectance value is given by

$$R = \left[\frac{n_a n_s - {n_{arc}}^2}{n_a n_s + {n_{arc}}^2}\right]^2 \quad (3)$$

Whereas for multilayer ARCs, the total reflection is calculated by considering the amount of light reflected from the interfaces between adjacent layers. For example, let i and j represent two adjacent layers. The reflection at the interface is given by the equation:

$$|R_{ij}| = (n_i - n_j)/(n_i + n_j),$$

and the phase difference is given by the equation:

$$\delta_i = 2\pi n_i d_i \cos\theta_i/\lambda \quad (4)$$

where d_i, θ_i, and λ are the thickness of the layer, the angle of refraction, and the wavelength of light, respectively. The total reflection across a multilayer ARC can then be expressed as a sum of reflections at each interface and is given by the following equation:

$$R_{tot} = R_{01} + R_{12} + R_{23} + R_{3s} \quad (5)$$

$$\text{where } R_{01} = |R_{01}|,\ R_{12} = |R_{12}|\exp(-2(\delta_1),\ R_{23} = |R_{23}|\exp(-2(\delta_1 + \delta_2))$$

$$\text{and } R_{34} = |R_{34}|\exp(-2(\delta_1 + \delta_2 + \delta_3))$$

Thus, by adjusting the material refractive index and precisely controlling each layer thickness, reflection loss can be minimized, optimizing the ARC and, in turn, enhancing the performance of PSCs.

For instance, in a recent publication of our group,[113] we demonstrated that precise determination of the refractive index is critical for achieving close agreement between experimental results and optical Modeling predictions. We introduced a new design strategy by combining two types of ARCs, planar and porous within a single graded-index ARC. The planar layers provide structural uniformity and mechanical stability, while the porous layers introduce controlled air voids, effectively lowering the local refractive index. By carefully integrating these two types of layers, the resulting graded-index ARC achieves a variation in refractive index, which significantly minimizes reflection across a broad wavelength range. This design approach allows for a reduction in reflection losses that is nearly twice as effective as that obtained with conventional planar, porous, or single-layer graded ARCs. By adjusting the deposition angle and layering sequence, we were able to lower the refractive index of MgF_2 beyond its standard value, a modification typically achievable only through solution-based processing (as illustrated in Fig. 6). This precise control over the refractive index not only enhances the optical performance of the ARC but also provides a versatile route for designing coatings with custom optical properties highlighting the importance of integrating structural engineering and advanced material processing techniques to optimize coating performance for next-generation optical and photovoltaic applications.

Further, with the increasing complexity of material systems and structural architectures, machine learning (ML) is also one of the emerging and powerful complement to optical modeling for accelerating the design and optimization of advanced ARCs. Through materials screening, ML models trained on experimental and simulation datasets can rapidly identify promising coating compositions and hybrid systems with desirable refractive indices, bandgap characteristics, and environmental stability, thereby significantly reducing reliance on trial-and-error experimentation. For multilayer and gradient-index ARCs, inverse design frameworks-based algorithms enable the direct prediction of optimal layer sequences, thicknesses, and material combinations that maximize broadband transmittance under specific angular and environmental constraints. Moreover, data-driven performance prediction models establish quantitative relationships between processing parameters, microstructural features, and optical, mechanical, and environmental properties, facilitating reliable lifetime assessment and degradation forecasting. Machine learning also supports multi-objective optimization by simultaneously considering optical efficiency, durability, cost, and scalability, allowing the identification of balanced design solutions that satisfy practical deployment requirements. When integrated with optical simulations, automated fabrication platforms, and real-time characterization systems, ML-driven approaches are expected to enable closed-loop optimization and autonomous materials discovery.

Wang *et al.*[114] demonstrated the automated design of multifunctional coatings that balance aesthetic and optical performance criteria for solar cells. Their approach enables the development of coatings that impart color to solar cells while minimizing efficiency losses, thereby enhancing both visual appeal and energy performance. Similarly, Oktay *et al.*[115] developed and evaluated a data-driven model based on a dataset of 3000 simulations to predict optical reflectance in multilayer

anti-reflective coatings (ARCs). These coatings were specifically designed for infrared sensing applications, where excessive reflection can significantly reduce detection sensitivity. Together, these studies illustrate a transformative pathway toward intelligent, adaptive, multifunctional, and sustainable ARC technologies that can be first designed and then experimentally realized for application in PSCs.

8. Conclusions

PSCs continue to demonstrate remarkable promise, and relatively simple light management strategies present an untapped opportunity to further push their efficiency and durability. Among these, ARCs stand out as one of the most practical and impactful solutions, acting on the optimisation of the device performances exploiting the light management. In addition to enhancing light harvesting, well-designed ARCs can also contribute to thermal regulation, mitigating performance losses under high temperatures, and provide self-cleaning and protective functions to extend device lifetime. Importantly, in some architectures, transparent electrodes can be engineered to serve dual roles as both electrodes and ARCs, reducing fabrication complexity. Indeed, even incremental efficiency gains of 1–2% from optimized ARCs are significant when considering large-scale deployment.

In our view, the future of ARCs in PSCs lies in multifunctionality. Optical enhancement alone is not enough. Scalable ARCs must also address stability, manufacturability, and cost-effectiveness. We believe the integration of machine learning and predictive Modeling will be transformative, enabling rapid exploration of material combinations and structural designs that traditional trial-and-error approaches cannot match. As PSCs move closer to commercialization, ARCs should not be treated as peripheral add-ons but as central components of device architecture. With continued innovation in multifunctional and scalable ARC technologies, PSCs have the potential to surpass current efficiency benchmarks, while ensuring long-term operational stability. With these advancements, ARCs could play a pivotal role in driving the next generation of high-efficiency, durable, and commercially viable PSCs.

Author contributions

Conceptualization: SR, SC, GG. Writing—original draft: SR. Writing—review & editing: SR, SC, GG.

Conflicts of interest

There are no conflicts to declare.

Data availability

No primary research results, software or code have been included and no new data were generated or analysed as part of this review.

Acknowledgements

The authors acknowledge the Fondazione Cariplo Economia Circolare 2021 Project “Green flexible hybrid perovskite solar module for the market: from smart lead manipulation to recycling” (FLHYPER, no 20201067), funded under the “Circular Economy-2020” call, the Ministero dell’Università e della Ricerca (MUR) and the University of Pavia through the program “Dipartimenti di Eccellenza 2023–2027".

Notes and references

1 A. O. M. Maka and J. M. Alabid, *Clean Energy*, 2022, **6**, 476–483.
2 S. Rani, A. Kumar and D. S. Ghosh, *Sol. RRL*, 2023, **7**, 2200863.
3 P. Holzhey, M. Prettl, S. Collavini, N. L. Chang and M. Saliba, *Joule*, 2023, **7**, 257–271.
4 A. S. R. Bati, Y. L. Zhong, P. L. Burn, M. K. Nazeeruddin, P. E. Shaw and M. Batmunkh, *Commun. Mater.*, 2023, **4**, 2.
5 S. Rani, A. Kumar and D. Sundar Ghosh, *Energy Technol.*, 2025, 2500438.
6 M. M. Tavakoli, K.-H. Tsui, Q. Zhang, J. He, Y. Yao, D. Li and Z. Fan, *ACS Nano*, 2015, **9**, 10287–10295.
7 S. Rani, A. Kumar, A. K. Chauhan and D. S. Ghosh, *J. Photonics Energy*, 2025, **15**, 015501.
8 Z. Zhang, Y. Feng, J. Ding, Q. Ma, H. Zhang, J. Zhang, M. Li, T. Geng, W. Gao, Y. Wang, B. Zhang, T. Pauporté, J.-X. Tang, H. Chen, J. Chen and C. Chen, *Nat. Commun.*, 2025, **16**, 753.
9 L. Shen, P. Song, K. Jiang, L. Zheng, J. Qiu, F. Li, Y. Huang, J. Yang, C. Tian, A. K.-Y. Jen, L. Xie and Z. Wei, *Nat. Commun.*, 2024, **15**, 10908.
10 C. Zuo, H. J. Bolink, H. Han, J. Huang, D. Cahen and L. Ding, *Adv. Sci.*, 2016, **3**, 1500324.
11 J. Y. Kim, J.-W. Lee, H. S. Jung, H. Shin and N.-G. Park, *Chem. Rev.*, 2020, **120**, 7867–7918.
12 H. S. Jung and N. Park, *Small*, 2015, **11**, 10–25.
13 Z. Xiong, Y.-S. Jeon, H. Wang, G. Fu, S.-H. Cho, S.-J. Chang, P. A. van Aken and N.-G. Park, *Adv. Mater.*, 2025, **37**, 2413712.
14 C. Zhang and N.-G. Park, *Commun. Mater.*, 2024, **5**, 194.
15 Z. Zaman, H. Shahroosvand, S. Bellani, F. Bonaccorso and M. K. Nazeeruddin, *Angew. Chem., Int. Ed.*, 2025, **64**, e202425191.
16 F. Berry, R. Mermet-Lyaudoz, J. M. Cuevas Davila, D. A. Djemmah, H. S. Nguyen, C. Seassal, E. Fourmond, C. Chevalier, M. Amara and E. Drouard, *Adv. Energy Mater.*, 2022, **12**, 2200505.
17 M. Krajewski, A. Callies, M. Heydarian, M. Heydarian, M. Hanser, P. S. C. Schulze, B. Bläsi and O. Höhn, *Adv. Mater. Interfaces*, 2023, **10**, 2300134.
18 Q. Lin, A. Armin, R. C. R. Nagiri, P. L. Burn and P. Meredith, *Nat. Photonics*, 2015, **9**, 106–112.
19 Q. Liu, P. Romero-Gomez, P. Mantilla-Perez, S. Colodrero, J. Toudert and J. Martorell, *Adv. Energy Mater.*, 2017, **7**(18), 1700356.

20 H. K. Raut, V. A. Ganesh, A. S. Nair and S. Ramakrishna, *Energy Environ. Sci.*, 2011, **4**(10), 3779–3804.
21 https://www.oxfordpv.com/tandem-cell-production.
22 https://sauletech.com/product/.
23 Q. Luo, X. Deng, C. Zhang, M. Yu, X. Zhou, Z. Wang, X. Chen and S. Huang, *Sol. Energy*, 2018, **169**, 128–135.
24 Y. Wang, H. Wang, M. Chen, P. Wang, Y. Mao, W. Han, T. Wang and D. Liu, *Sci. China Mater.*, 2021, **64**, 789–797.
25 X. Li, J. Gao, L. Xue and Y. Han, *Adv. Funct. Mater.*, 2010, **20**, 259–265.
26 J. Fu, M. Lu, Z. Wang, P. Hou, J. Lu, Y. Xie, S. Tian, X. Zhao and J. Solgel, *Sci. Technol.*, 2024, **111**, 395–408.
27 B. Aïssa, M. I. Hossain, A. Zekri, A. A. Abdallah and V. B. Benito, *Sol. Energy*, 2025, **293**, 113485.
28 K. H. Nielsen, S. Karlsson, R. Limbach and L. Wondraczek, *Sci. Rep.*, 2015, **5**, 17708.
29 M. I. Hossain, A. Ali, V. Bermudez Benito, B. Figgis and B. Aïssa, *Materials*, 2022, **15**(20), 7139.
30 G. Perrakis, A. C. Tasolamprou, G. Kakavelakis, K. Petridis, M. Graetzel, G. Kenanakis, S. Tzortzakis and M. Kafesaki, *Sci. Rep.*, 2024, **14**, 548.
31 A. S. Sarkın, N. Ekren and Ş. Sağlam, *Sol. Energy*, 2020, **199**, 63–73.
32 M. I. Hossain, B. Aïssa, A. Samara, S. A. Mansour, C. A. Broussillou and V. B. Benito, *ACS Omega*, 2021, **6**, 5276–5286.
33 M. I Hossain, G. Al Kubaisi, B. Aïssa and S. Mansour, *Mater. Sci. Technol.*, 2022, **38**, 753–759.
34 M. Z. Khan, C. Pfau, M. Schak, P.-T. Miclea, V. Naumann, A. Debess, C. Hagendorf and K. Ilse, *J. Renewable Sustainable Energy*, 2020, **12**, 053504.
35 M. Modaresialam, Z. Chehadi, T. Bottein, M. Abbarchi and D. Grosso, *Chem. Mater.*, 2021, **33**, 5464–5482.
36 Q. Luo, X. Deng, C. Zhang, M. Yu, X. Zhou, Z. Wang, X. Chen and S. Huang, *Sol. Energy*, 2018, **169**, 128–135.
37 S.-I. Park, Y. Quan, S.-H. Kim, H. Kim, S. Kim, D.-M. Chun, C. Lee, M. Taya, W.-S. Chu and S.-H. Ahn, *Int. J. Precis. Eng. Manuf. - Green Technol.*, 2016, **3**, 397–421.
38 C. Wang, S. Yu, X. Guo, T. Kearney, P. Guo, R. Chang, J. Chen, W. Chen and C. Sun, *Cell Rep. Phys. Sci.*, 2020, **1**, 100108.
39 M. Lu, Q. Liu, Z. Wang, X. Zhang, G. Luo, J. Lu, D. Zeng, X. Zhao and S. Tian, *Mater. Today Chem.*, 2023, **29**, 101473.
40 C. M. Esteban, R. Sharma, W. Lee, J. Ji and S. Yoo, *ACS Appl. Polym. Mater.*, 2025, **7**, 1471–1480.
41 B. Xiao, Y. Qian, X. Li, Y. Tao, Z. Yi, Q. Jiang, Y. Luo and J. Yang, *J. Energy Chem.*, 2023, **76**, 259–265.
42 S. B. Khan, S. Irfan and Z. Zhang, *J. Mater. Res. Technol.*, 2024, **31**, 1616–1625.
43 D. Adak, R. Bhattacharyya and H. C. Barshilia, *Renewable Sustainable Energy Rev.*, 2022, **159**, 112145.
44 T. Faravelli, M. Pinciroli, F. Pisano, G. Bozzano, M. Dente and E. Ranzi, *J. Anal. Appl. Pyrolysis*, 2001, **60**, 103–121.
45 M. Kim, G.-H. Kim, K. S. Oh, Y. Jo, H. Yoon, K.-H. Kim, H. Lee, J. Y. Kim and D. S. Kim, *ACS Nano*, 2017, **11**, 6057–6064.
46 C. J. Ruud, A. Cleri, J.-P. Maria and N. C. Giebink, *Nano Lett.*, 2022, **22**, 7358–7362.
47 W. Li, W. Cao, H. Zhou, X. Zhang and K. Wang, *RSC Adv.*, 2024, **14**, 2757–2762.
48 M. A. Zahid, H. Park, Y. H. Cho and J. Yi, *Small Struct.*, 2021, **112**, 110813.
49 X. Sun, X. Xu, G. Song, J. Tu, L. Li, P. Yan, W. Zhang and K. Hu, *Small Struct.*, 2020, **101**, 109739.
50 W. A. A. Syed, N. Rafiq, A. Ali, R. Din and W. H. Shah, *Optik*, 2017, **136**, 564–572.
51 D. B. Mahadik, R. V Lakshmi and H. C. Barshilia, *Sol. Energy Mater. Sol. Cells*, 2015, **140**, 61–68.
52 W. Zhang, J. Tu, W. Long, W. Lai, Y. Sheng and T. Guo, *Energy Procedia*, 2017, **130**, 72–76.
53 A. S. Rad, A. Afshar and M. Azadeh, *Small Struct.*, 2020, **107**, 110027.
54 D. Ha, Z. Fang, L. Hu and J. N. Munday, *Adv. Energy Mater.*, 2014, **4**, 1301804.
55 R. Prado, G. Beobide, A. Marcaide, J. Goikoetxea and A. Aranzabe, *Sol. Energy Mater. Sol. Cells*, 2010, **94**, 1081–1088.
56 https://refractiveindex.info/?shelf=main&book=LiF&page=Li.
57 https://refractiveindex.info/?shelf=main&book=MgF2&page=Dodge-o.
58 A. Kumar, S. Rani and D. Sundar Ghosh, *Sol. Energy Mater. Sol. Cells*, 2024, **268**, 112737.
59 A. Paliwal, K. P. S. Zanoni, C. Roldán-Carmona, N. Rodkey and H. J. Bolink, *ACS Energy Lett.*, 2024, **9**, 4587–4595.
60 F. Ye, T. Wu, Z. Zhu, Z. Chen, H. Wang, J. Liang, M. Xiao, C. Tao and G. Fang, *Nanotechnology*, 2020, **31**, 275407.
61 D. I. Kim, S. Lee, S. Ji, S. Kang, W. Song, S. Myung, S. Yim, S. S. Lee and K.-S. An, *Small Struct.*, 2024, **5**, 2300338.
62 X. Wang, W. Wang, J. Liu, J. Qi, Y. He, Y. Wang, W. Hu, Y. Cheng, K. Chen, Y. Hu, A. Mei and H. Han, *Adv. Funct. Mater.*, 2022, **32**, 2203872.
63 B. Dudem, I. S. Jin, A. R. Mule, J. W. Jung and J. S. Yu, *ACS Sustain. Chem. Eng.*, 2019, **7**, 12981–12989.
64 J. S. Choi, Y. W. Jang, U. Kim, M. Choi and S. M. Kang, *Adv. Energy Mater.*, 2022, **12**(33), 2201520.
65 X. Lang, Z. Gao, Y. Zhao, Y. Jiang, X. Liu, M. Li, Y. Gou, C. Chen, D. Zhao, C. Wang, X. Han, J. Ye and C. Xiao, *ACS Appl. Energy Mater.*, 2024, **7**, 11670–11677.
66 H. Yao and Q. Tang, *Sol. Energy*, 2020, **211**, 446–452.
67 J. Y. Huang, Y. Wang, G. T. Fei, S. H. Xu, B. Wang and Z. Zeng, *Colloids Surf., A*, 2022, **652**, 129907.
68 R. Datt, S. Bishnoi, D. Hughes, P. Mahajan, A. Singh, R. Gupta, S. Arya, V. Gupta and W. C. Tsoi, *Sol. RRL*, 2022, **6**, 2200266.
69 Z. Shi, D. Zhou, X. Zhuang, W. Xu, S. Liu, Y. Liao, P. Jia, G. Pan, W. Liu, J. Zhu and H. Song, *Adv. Energy Mater.*, 2024, **14**, 2303735.
70 C. W. Kim, T. Y. Eom, I. S. Yang, B. S. Kim, W. I. Lee, Y. S. Kang and Y. S. Kang, *Sci. Rep.*, 2017, **7**, 6849.
71 J. Jia, J. Dong, J. Lin, Z. Lan, L. Fan and J. Wu, *J. Mater. Chem. C*, 2019, **7**, 937–942.

72 F. Bella, G. Griffini, J.-P. Correa-Baena, G. Saracco, M. Grätzel, A. Hagfeldt, S. Turri and C. Gerbaldi, *Science*, 2016, **354**, 203–206.
73 M. M. Tavakoli, H. T. Dastjerdi, D. Prochowicz, P. Yadav, R. Tavakoli, M. Saliba and Z. Fan, *J. Mater. Chem. A*, 2019, **7**, 14753–14760.
74 H. Bian, Q. Wang, S. Yang, C. Yan, H. Wang, L. Liang, Z. Jin, G. Wang and S. F. Liu, *J. Mater. Chem. A*, 2019, **7**, 5740–5747.
75 C. Y. Xu, W. Hu, G. Wang, L. Niu, A. M. Elseman, L. Liao, Y. Yao, G. Xu, L. Luo, D. Liu, G. Zhou, P. Li and Q. Song, *ACS Nano*, 2020, **14**, 196–203.
76 J. Wang, H. Zhang, L. Wang, K. Yang, L. Cang, X. Liu and W. Huang, *ACS Appl. Energy Mater.*, 2020, **3**, 4484–4491.
77 E. Cho, Y. Y. Kim, D. S. Ham, J. H. Lee, J.-S. Park, J. Seo and S.-J. Lee, *Nano Energy*, 2021, **82**, 105737.
78 X. Zhang, Z. Wang, P. Hou, S. Wu, J. Lu, X. Zhao and S. Tian, *Nanoscale*, 2024, **16**, 9617–9624.
79 S.-K. Jung, K. Park, D.-K. Lee, J.-H. Lee, H. Ahn and J.-W. Lee, *Nanotechnology*, 2024, **35**, 135401.
80 B. Dudem, J. H. Heo, J. W. Leem, J. S. Yu and S. H. Im, *J. Mater. Chem. A*, 2016, **4**, 7573–7579.
81 D. I. Kim, J. W. Lee, R. H. Jeong, J. W. Yang, S. Park and J.-H. Boo, *Energy*, 2020, **210**, 118582.
82 S. Bachevillier, H.-K. Yuan, A. Strang, A. Levitsky, G. L. Frey, A. Hafner, D. D. C. Bradley, P. N. Stavrinou and N. Stingelin, *Adv. Funct. Mater.*, 2019, **29**, 1808152.
83 K. Ilse, L. Micheli, B. W. Figgis, K. Lange, D. Daßler, H. Hanifi, F. Wolfertstetter, V. Naumann, C. Hagendorf, R. Gottschalg and J. Bagdahn, *Cell Press*, 2019, **3**, 2303–2321.
84 P. M. Martin-Sanchez, C. Gebhardt, J. Toepel, J. Barry, N. Munzke, J. Günster and A. A. Gorbushina, *Int. Biodeterior. Biodegrad.*, 2018, **129**, 13–22.
85 R. Conceição, H. G. Silva, J. Mirão and M. Collares-Pereira, *Energies*, 2018, **11**, 294.
86 M. A. Shirakawa, R. Zilles, A. Mocelin, C. C. Gaylarde, A. Gorbushina, G. Heidrich, M. C. Giudice, G. M. B. Del Negro and V. M. John, *J. Environ. Manage.*, 2015, **157**, 160–167.
87 M. Kim, T.-W. Kang, S. H. Kim, E. H. Jung, H. H. Park, J. Seo and S.-J. Lee, *Sol. Energy Mater. Sol. Cells*, 2019, **191**, 55–61.
88 R. A. Maniyara, V. K. Mkhitaryan, T. L. Chen, D. S. Ghosh and V. Pruneri, *Nat. Commun.*, 2016, **7**, 13771.
89 G. Perrakis, A. C. Tasolamprou, G. Kakavelakis, K. Petridis, M. Graetzel, G. Kenanakis, S. Tzortzakis and M. Kafesaki, *Sci. Rep.*, 2024, **14**, 548.
90 G. Womack, K. Isbilir, F. Lisco, G. Durand, A. Taylor and J. M. Walls, *Surf. Coat. Technol.*, 2019, **358**, 76–83.
91 A. Elsafi, B. Aïssa, K. Ilse and A. Abdallah, *Sol. Energy*, 2025, **293**, 113446.
92 N. Ammari, M. Mehdi, A. Alami Merrouni and A. Benazzouz, *Sustain. Energy Technol. Assess.*, 2023, **60**, 103547.
93 P. Wang, X. Yan, J. Zeng, C. Luo and C. Wang, *Appl. Surf. Sci.*, 2022, **602**, 154408.
94 G. Zhang, B. Zhou, J. Luo, Q. Wei, C. Li, J. Tang, J. Wang, X. Wen and Y. Yang, *ACS Sustain. Chem. Eng.*, 2025, **13**, 20030–20041.
95 Y. Demirhan, *Opt. Quantum Electron.*, 2026, **58**, 75.
96 A. M. Law, L. O. Jones and J. M. Walls, *Sol. Energy*, 2023, **261**, 85–95.
97 U. Mehmood, F. A. Al-Sulaiman, B. S. Yilbas, B. Salhi, S. H. A. Ahmed and M. K. Hossain, *Sol. Energy Mater. Sol. Cells*, 2016, **157**, 604–623.
98 L. Zhang, J. Xu, Z. Hu, P. Wang, J. Shang, J. Zhou and L. Ren, *ACS Appl. Mater. Interfaces*, 2024, **16**, 38690–38701.
99 R. Suzuki and J. Solgel, *Sci. Technol.*, 2023, **106**, 860–868.
100 R. A. Sathya and C. Ponraj, *Mater. Chem. Phys.*, 2025, **341**, 130880.
101 J. Sun, X. Wang, J. Wu, C. Jiang, J. Shen, M. A. Cooper, X. Zheng, Y. Liu, Z. Yang and D. Wu, *Sci. Rep.*, 2018, **8**, 5438.
102 K. Isakov, C. Kauppinen, S. Franssila and H. Lipsanen, *ACS Appl. Mater. Interfaces*, 2020, **12**, 49957–49962.
103 S. Rani, A. Kumar and D. S. Ghosh, *IEEE J. Photovolt.*, 2022, **12**, 595–601.
104 C. C. Katsidis and D. I. Siapkas, *Appl. Opt.*, 2002, **41**, 3978–3987.
105 N. Sahouane and A. Zerga, *Energy Procedia*, 2014, **44**, 118–125.
106 A.-K. S. O. Hassan, A. S. A. Mohamed, M. M. T. Maghrabi and N. H. Rafat, *Appl. Opt.*, 2015, **54**, 1399–1409.
107 A. Kumar, S. Rani and D. Sundar Ghosh, *Mater. Today: Proc.*, 2022, **66**, 3265–3268.
108 A. Kumar, S. Rani, N. Chandrakar and D. Sundar Ghosh, *Mater. Today: Proc.*, 2023, **72**, 2460–2466.
109 S. Rani, D. Kuar, V. Jeyachandran and D. S. Ghosh, *Small Struct.*, 2022, **131**, 112612.
110 S. Guruprasad, S. Rani, A. Malik, P. Basumatary and D. Sundar Ghosh, *Energy Technol.*, 2025, 2500608.
111 A. Malik, S. Rani, S. Guruprasad, P. Basumatary and D. S. Ghosh, *Adv. Theory Simul.*, 2025, e00179.
112 A. Kumar, S. Rani and D. Sundar Ghosh, *Small Struct.*, 2023, **145**, 114409.
113 S. Rani, F. Toniolo, S. Cavalli, M. Degani, L. Ghidoni, M. Faverzani, A. Girella, L. C. Andreani, P. Biagioni, A. Taglietti, C. Milanese and G. Grancini, *ACS Appl. Energy Mater.*, 2026, **9**, 1346–1353.
114 C. Wang, K. Lu, C. Li, L. Ma, X. Li and Y. Zhou, *Renewable Energy*, 2025, **249**, 123160.
115 S. Oktay, İ. Duru, H. Bakır and T. E. Tabaru, *Opt. Quantum Electron.*, 2025, **57**, 101.